Article

Immunity

Microbiota translocation following intestinal barrier disruption promotes Mincle-mediated training of myeloid progenitors in the bone marrow

Graphical abstract

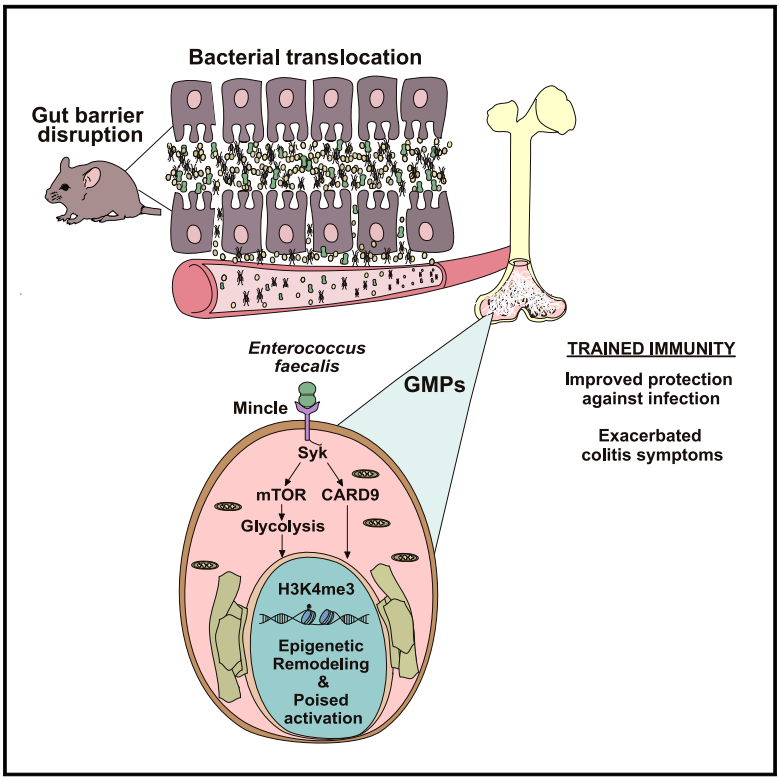

Authors

Iñaki Robles-Vera, Aitor Jarit-Cabanillas, Paola Brandi, ..., José Luis Subiza, Salvador Iborra, David Sancho

Correspondence

inaki.robles@cnic.es (I.R.-V.), dsancho@cnic.es (D.S.)

In brief

Robles-Vera et al. unveil the capacity of gut microbiota translocation, particularly *Enterococcus faecalis*, to mediate a Mincle-dependent induction of trained immunity in myeloid bone marrow progenitors. This can be protective against subsequent infection but may also mediate a detrimental inflammatory response linked to colitis.

Highlights

- Gut barrier disruption induces trained immunity in bone marrow progenitors
- *Enterococcus faecalis* translocates to the bone marrow, inducing trained immunity
- Mincle sensing of *E. faecalis* mediates trained immunity of bone marrow progenitors
- Mincle-mediated trained immunity protects against infection but worsens inflammation

Robles-Vera et al., 2025, Immunity *58*, 381–396
February 11, 2025
https://doi.org/10.1016/j.immuni.2024.12.012

CellPress

Immunity

CellPress
OPEN ACCESS

Article

Microbiota translocation following intestinal barrier disruption promotes Mincle-mediated training of myeloid progenitors in the bone marrow

Iñaki Robles-Vera,[1,*] Aitor Jarit-Cabanillas,[1,5] Paola Brandi,[1,7] María Martínez-López,[1,8] Sarai Martínez-Cano,[1,2] Manuel Rodrigo-Tapias,[1] Marcos Femenía-Muiña,[1] Ana Redondo-Urzainqui,[1] Vanesa Nuñez,[1] Cristina González-Correa,[3] Javier Moleón,[3] Juan Duarte,[3] Laura Conejero,[2] Pablo Mata-Martínez,[4] Carmen María Díez-Rivero,[2] Marta Bergón-Gutiérrez,[4] Iván Fernández-López,[1] Manuel J. Gómez,[1] Ana Quintas,[1] Ana Dopazo,[1] Fátima Sánchez-Cabo,[1] Esther Pariente,[1] Carlos del Fresno,[4] José Luis Subiza,[2] Salvador Iborra,[5,6] and David Sancho[1,9,*]

[1]Centro Nacional de Investigaciones Cardiovasculares (CNIC), Madrid, Spain
[2]Inmunotek S.L., Alcalá de Henares, Spain
[3]Department of Pharmacology, School of Pharmacy, University of Granada, IBS-Granada, Centro de Investigaciones Biomédicas (CIBM), CIBER-Enfermedades Cardiovasculares (CiberCV), Granada, Spain
[4]Immunomodulation Lab, Innate Immune Response Group, IdiPAZ, La Paz University Hospital, Madrid, Spain
[5]Department of Immunology, Ophthalmology and ENT, School of Medicine, Universidad Complutense de Madrid, 12 de Octubre Health Research Institute (imas12), Madrid, Spain
[6]Fundación Inmunotek, Alcalá de Henares, Spain
[7]Present address: Telethon Institute of Genetics and Medicine (TIGEM), Pozzuoli, Italy
[8]Present address: Champalimaud Research, Champalimaud Centre for the Unknown, Lisbon, Portugal
[9]Lead contact
*Correspondence: inaki.robles@cnic.es (I.R.-V.), dsancho@cnic.es (D.S.)
https://doi.org/10.1016/j.immuni.2024.12.012

SUMMARY

Impairment of the intestinal barrier allows the systemic translocation of commensal bacteria, inducing a proinflammatory state in the host. Here, we investigated innate immune responses following increased gut permeability upon administration of dextran sulfate sodium (DSS) in mice. We found that *Enterococcus faecalis* translocated to the bone marrow following DSS treatment and induced trained immunity (TI) hallmarks in bone-marrow-derived mouse macrophages and human monocytes. DSS treatment or heat-killed *E. faecalis* reprogrammed bone marrow progenitors (BMPs), resulting in enhanced inflammatory responses *in vitro* and *in vivo* and protection against subsequent pathogen infections. The C-type lectin receptor Mincle (*Clec4e*) was essential for *E. faecalis*-induced TI in BMPs. *Clec4e*$^{-/-}$ mice showed impaired TI upon *E. faecalis* administration and reduced pathology following DSS treatment. Thus, Mincle sensing of *E. faecalis* induces TI that may have long-term effects on pathologies associated with increased gut permeability.

INTRODUCTION

The host immune system has coevolved with trillions of microorganisms, drawing a fine balance between resistance to pathogens while maintaining symbiosis with commensal microbiota. However, imbalances in gut microbial composition or in its containment can contribute to inflammatory disorders.[1–3] Sensing of microbial signals by myeloid cells may lead to metabolic and epigenetic reprogramming that boosts inflammatory responses to secondary challenges and induces protection toward pathogen re-infection, a process termed trained immunity (TI).[4,5] These transient epigenetic changes can be mediated by microbe-derived metabolites such as short-chain fatty acids (SCFAs) through their effects on histone-modifying enzymes.[6,7] Moreover, metabolic changes resulting from alterations in the gut microbiota affect the bone marrow (BM) niche.[8] In contrast to germ-free (GF) mice, mice harboring gut microbiota show increased myelopoiesis.[9–11]

The long-term effects of TI are explained by the modulation of BM progenitors (BMPs).[12] Among the receptors sensing microbial signals, Dectin-1 is a paradigmatic C-type lectin receptor (CLR) that drives TI.[13] Mincle (*Clec4e*) is a closely related CLR that shares similar signaling pathways with Dectin-1[14] and senses ligands in different microbes[15] but has not been previously related to TI. Mincle mediates sensing of ligands in microbiota by myeloid cells, promoting intestinal barrier integrity.[16] Increased gut permeability leading to bacterial translocation can arise after exposure to certain diet components, medications, alcohol, radiation, and hyperglycemia or as a consequence of various pathologies.[17–20] Systemic dissemination of gut microbiota, microbial products, and microbe-derived metabolites that reach the circulation result in immune cell activation.

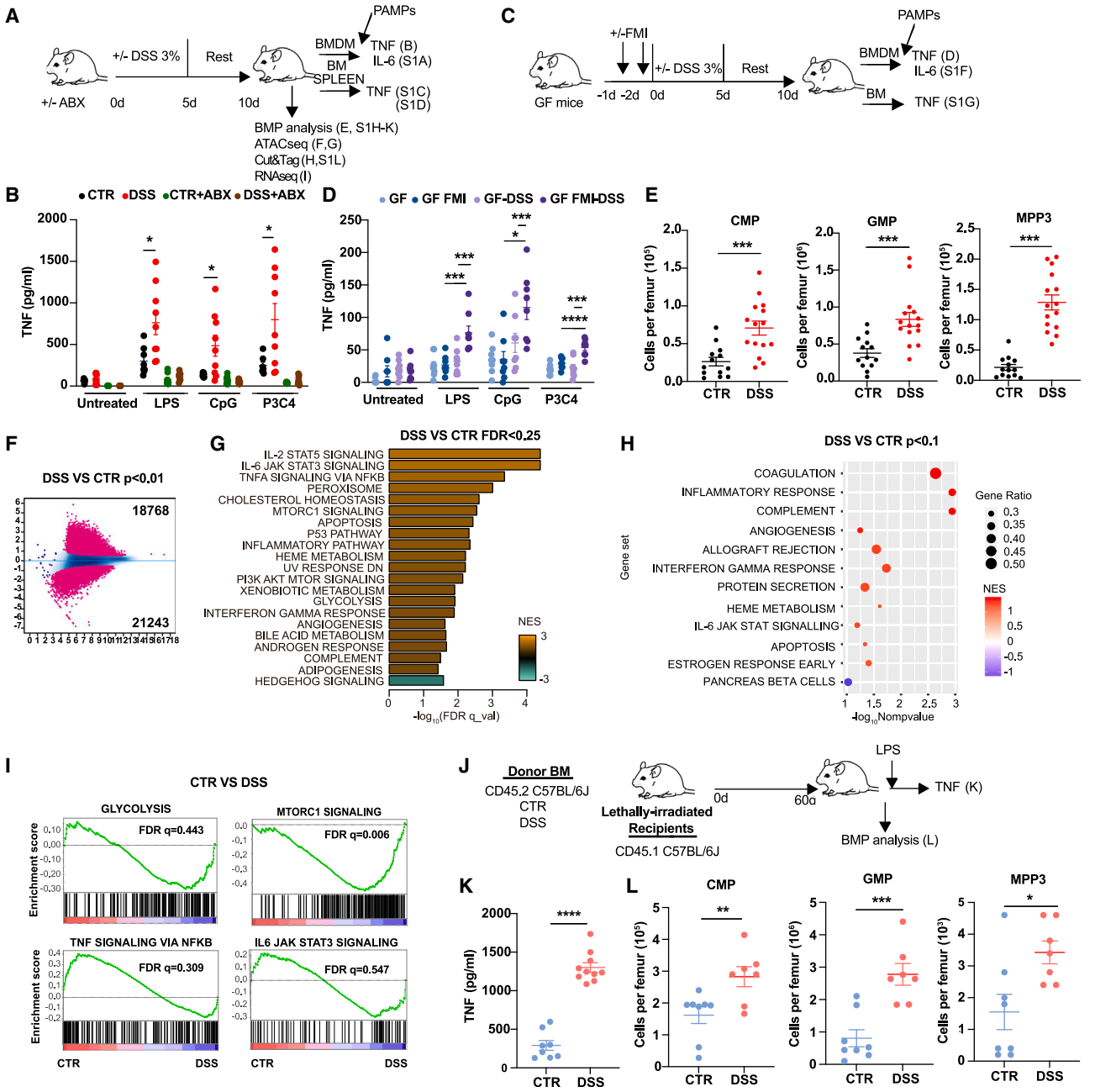

Figure 1. Gut microbiota translocation induces trained immunity in myeloid bone marrow progenitors

(A and B) (A) Mice were treated or not with DSS and antibiotics (ABX) as indicated in the outline; bone marrow (BM) extracted and BM-derived macrophages (BMDMs) generated and stimulated for 24 h with the following pathogen-associated molecular patterns: LPS, CpG, or Pam3CSK4 (P3C4). (B) TNF production measured by ELISA in culture supernatant of BMDMs from the indicated treatments and stimulations. Data obtained from a pool of two independent experiments (n = 7–9).

(C and D) (C) Germ-free (GF) mice were administered or not with fecal microbiota inoculation (FMI) from SPF mice and treated or not with the DSS protocol as indicated. Then, BMDMs were generated and stimulated as in (A).

(D) TNF production measured by ELISA in culture supernatant of BMDMs from indicated treatments and stimulations. Two pooled independent experiments (n = 8).

(E) Mice were treated or not with DSS, as indicated in (A), and BM myeloid progenitors (BMPs) counted at day 10. Graphs show total numbers per femur of common myeloid progenitors (CMPs), granulocyte-monocyte progenitors (GMPs), and multipotent progenitor cells (MPP3). Three pooled independent experiments (n = 13–15).

(F and G) ATAC-seq analysis in GMPs sorted from BM of control (CTR) or DSS mice at day 10 of the protocol shown in (A). (F) MAplot showing 40.011 differentially accessible peaks between DSS and CTR mice GMPs, with $p < 0.01$. (G) Bar plot showing enriched gene sets from the MSigDB Hallmark collection with false discovery rate (FDR) < 0.25. Positive normalized enrichment score (NES) values (orange color) and negative (green color) indicate congruent over- or

(legend continued on next page)

However, the link between microbiota translocation and TI remains unresolved.[21–24]

We sought to examine the impacts of microbial dissemination as a result of colitis injury in distant immune sites and cells. To explore mechanisms connecting gut microbiota translocation with systemic inflammation we administered dextran sulfate sodium (DSS) in mice, which impairs the intestinal barrier, and we found translocation of gut commensals to distal tissues, including the BM. This microbiota translocation drove epigenetic changes and promoted TI in BMPs. *Enterococcus faecalis* (*E. faecalis*) was one of the bacteria identified in the BM that activated immune cells in a Mincle-dependent manner. Consistently, *Clec4e*$^{-/-}$ mice showed reduced TI-related inflammation and pathology upon *E. faecalis* administration or DSS treatment. Our results identify Mincle sensing of gut microbiota translocation (including *E. faecalis* but potentially also other species such as *Staphylococcus aureus*) as an inducer of TI, which can subsequently enhance the inflammatory response, leading to protective or detrimental effects.

RESULTS

Gut barrier disruption induces TI in myeloid BMPs

Acute colitis induced by DSS treatment causes gut permeability and massive translocation of gut microbiota to distal tissues.[25] We therefore examined how gut microbiota translocation impacted innate immune cell responses to secondary stimulation. Mice were treated with antibiotics (ABXs) that reduce gut microbiota[26] and given 3% DSS in drinking water for 5 days, with PBS and normal drinking water controls. After a 5-day or 15-day rest period for epithelial repair, BM cells were collected (Figures 1A, S1A, and S1B). BM-derived macrophages (BMDMs) obtained from DSS-treated mice ("DSS mice" onward) showed an increased production of tumor necrosis factor (TNF) and interleukin-6 (IL-6) when stimulated with either LPS (TLR4 ligand), CpG (TLR9 ligand), or Pam3Csk4 (P3C4, TLR1/2 ligand) compared with untreated mice. ABX treatment abolished this effect (Figures 1B and S1A). Moreover, these enhanced secondary responses occurred in BMDMs from *Rag1*$^{-/-}$ mice (Figure S1C), suggesting that this effect is independent of the adaptive immunity. Total BM cells from DSS mice also showed boosted response against secondary challenges *ex vivo*, which was prevented upon ABX administration (Figure S1D). In addition, splenic macrophages and neutrophils from DSS mice also displayed boosted TNF production in peripheral organs compared with untreated controls (Figure S1E). GF C57BL/6 mice administered a fecal microbiota inoculation (FMI) to restore the conventional gut microbiota, followed by DSS treatment (Figure 1C) showed increased TNF and IL-6 production by BMDMs (Figures 1D and S1F) and increased TNF by total BM (Figure S1G) upon pathogen-associated molecular pattern restimulation compared with GF mice that did not receive FMI or DSS. This further confirms the role of gut microbiota in BM reprogramming.

DSS treatment led to the expansion of various BMPs, such as common myeloid progenitors (CMPs), granulocyte-monocyte progenitors (GMPs), multipotent progenitor 3 (MPP3) and MPP4 cells, and long-term (LT), but not short-term (ST), hematopoietic stem cells (HSCs) (Figures 1E and S1H–S1K). To determine whether this shift in BMPs was due to an intrinsic epigenetic and/or transcriptional reprogramming in the BMPs, we sorted GMPs from DSS or untreated mice and analyzed: (1) chromatin accessibility by assay for transposase-accessible chromatin with sequencing (ATAC-seq); (2) H3K4me3 by Cut&Tag, indicating open and potentially active promoter regions linked to TI[27]; and (3) gene expression by RNA sequencing (RNA-seq). Our ATAC-seq results revealed deep changes in chromatin accessibility in GMPs from DSS mice compared with untreated controls (Figure 1F). By ascribing open regions to gene promoters, gene set enrichment analysis (GSEA) showed an enrichment in pathways related to inflammation status, such as nuclear factor κB (NF-κB), proinflammatory cytokines, mTOR signaling, and pathways related to glycolysis (Figure 1G). Cut&Tag analysis showed a higher number of H3K4me3 counts in GMPs from DSS mice (Figure S1L). Additionally, GSEA from Cut&Tag sequencing showed an enrichment in similar pathways to those identified by ATAC-seq (Figure 1H). In contrast, GSEA on RNA-seq showed increased transcriptional activity in mTORC1 signaling, but not in inflammatory genes, in DSS mice compared with control mice (Figure 1I), suggesting that TI induces epigenetic changes but maintains a transcriptional resting state in inflammatory genes.[5]

To determine whether intrinsic epigenetic changes in BMPs drive TI in DSS mice, BM from CD45.2^{+} DSS or untreated donor mice was grafted into lethally irradiated CD45.1^{+} recipient mice. 60 days later, LPS challenge showed higher systemic TNF production in mice grafted with BM from DSS donors compared with untreated ones (Figures 1J and 1K). Moreover, myeloid BMPs (CMP, GMP, and MPP3) were expanded in mice grafted with BM from DSS donors compared with untreated donors (Figure 1L). These findings indicate that DSS, which promotes gut permeability and microbiota translocation,[28] induces epigenetic

under-expression of a pathway or function-associated genes in DSS compared with CTR condition. Only the top 20 hits (according to FDR) are represented. A pool of 3 mice was used per biological replicate, and 3 biological replicates were used per condition.
(H) H3K4me3 Cut&Tag analysis in GMPs sorted from BM of CTR or DSS mice at day 10 of protocol shown in (A). Bubble plot showing gene set enrichment analysis (GSEA) from the MSigDB Hallmark collection with $p < 0.1$. Positive NES values (red) and negative (purple) indicate congruent over- or under-expression of a pathway or function-associated genes in DSS compared with CTR condition. Only the top 20 hits (according to FDR) are represented. A pool of 3 mice was used per biological replicate, and 3 biological replicates were used per condition.
(I) RNA-seq analysis in GMPs obtained from untreated or DSS mice after DSS protocol described in (A). GSEA profile from gene expression changes in glycolysis, mTOR, IL-6, and TNF is highlighted. A pool of 3 mice was used per biological replicate, and 3 biological replicates were used per condition.
(J) Donor mice were treated or not with DSS as in (A) and BM grafted to CD45.1 C57BL/6J recipient mice.
(K) After 60 days, mice were challenged with LPS and TNF measured in plasma by ELISA 1 h later. Two pooled experiments (n = 8–10).
(L) Graphs show total numbers per femur of the indicated myeloid BMPs. Two pooled experiments (n = 7–8).
(B, D, E, K, and L) Individual data and mean ± SEM are shown. *$p < 0.05$; **$p < 0.01$; ***$p < 0.005$; ****$p < 0.001$ (unpaired Student's t test).
See also Figure S1.

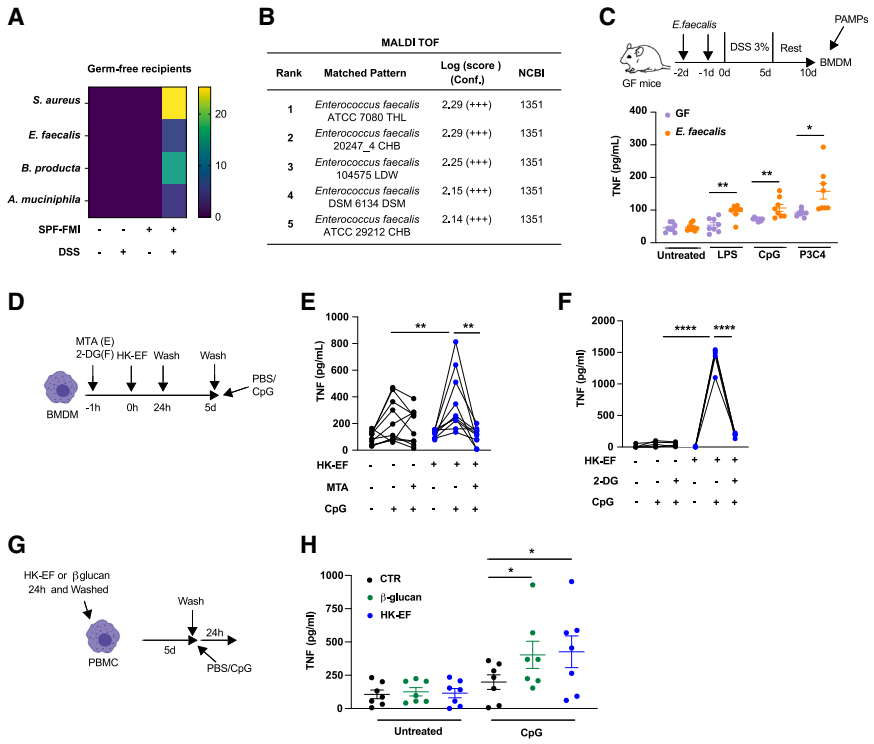

Figure 2. Identification of *Enterococcus faecalis* as a driver of bone marrow training upon gut barrier disruption

(A and B) BM from DSS mice was flushed and analyzed by 16S sequencing (A) or cultured in lysogeny broth (LB) plates for MALDI-TOF analysis (B). (A) Heatmap representing the bacterial read counts found in flushed BM. (B) MALDI biotyper report showing the species of bacteria detected by MALDI-TOF analysis from colonies obtained from LB plates in aerobic conditions after BM flushing. A log score of $\geq$1.80 represents high confidence and it is accepted for bacterial identification.

(C) GF mice were monocolonized or not with *E. faecalis* and treated with DSS; BM extracted and BMDMs generated and stimulated with LPS, CpG, or P3C4 for 24 h. TNF production measured by ELISA in culture supernatant of BMDMs from indicated treatments and stimulations. Two pooled experiments (n = 8).

(D–F) BMDMs obtained from C57BL/6J mice were pretreated or not with the methyltransferase inhibitor, 5′-methylthioadenosine (MTA) (E), or the glycolysis inhibitor 2-deoxy-glucose (2-DG) (F), for 1 h before incubation with HK-EF for a further 24 h. After this time, media were changed, and cells were rested for 5 days. TNF production measured by ELISA in culture supernatant of BMDMs after 24 h stimulation with CpG. (E) Three pooled experiments (n = 10). (F) Two pooled experiments (n = 5).

(G and H) Human peripheral blood mononuclear cells (PBMCs) were incubated for 24 h with or without β-glucan or HK-EF, washed and left resting for 5 days before restimulation with CpG. (H) TNF concentration was measured in the supernatant by ELISA. Two pooled experiments (n = 7).

(C and H) Individual data and mean ± SEM are shown. Unpaired Student's t test. (E and F) Individual data and paired Student's t test. *p < 0.05; **p < 0.01; ****p < 0.001.

See also Figures S2 and S3.

reprogramming of BMPs. This leads to a long-lasting state poised for inflammation that can be transferred by BM graft, thus meeting key hallmarks of TI.

Bacteria translocate to the BM and promote TI upon gut barrier disruption

Following DSS treatment, we found ABX-sensitive bacteria under anaerobic and aerobic culture conditions not only in the liver but also in the BM (Figures S2A and S2B). Unbiased 16S-rRNA sequencing of bacteria in the BM from GF mice, receiving or not receiving FMI from specific pathogen-free (SPF) mice, and exposed or not to DSS, revealed four bacterial species translocating to the BM from the gut: *Staphylococcus aureus*, *Enterococcus faecalis*, *Blautia producta*, and *Akkermansia muciniphila* (Figure 2A). The culture of BM flushed from DSS mice in a rich medium for broad-spectrum bacteria revealed one type of morphologically homogeneous colony facultative anaerobic, Gram^{+}, MacConkey^{neg}, Aesculin^{+}, and validated by analytical profile index test as *Enterococcus sp.* (*E. faecalis* 99.3%) (Figures S2C and S2D). Matrix-assisted laser desorption ionization time-of-flight (MALDI-TOF) mass spectrometry analysis confirmed *E. faecalis* as the only bacteria detected upon culture of BM from DSS mice in rich medium (Figure 2B). The quantification of *E. faecalis* cultured from the BM of one tibia and femur revealed an average of 2 × 10^2 colony-forming units (CFUs), growing similarly in aerobic and anaerobic conditions (Figure S2E).

Next, we tested the intrinsic capacity of *E. faecalis* translocation to induce TI. To this aim, GF mice were monocolonized with 10^8 CFU *E. faecalis* for two consecutive days prior to DSS administration (Figure 2C). The monocolonization with *E. faecalis* induced enhanced TNF and IL-6 production by BMDMs upon rechallenge with LPS, CpG, and P3C4 (Figures 2C and S2F). To assess the ability of heat-killed *E. faecalis* (HK-EF) to induce TI hallmarks *in vitro*, we treated BMDMs for 24 h with HK-EF in the presence of 5′-methylthioadenosine (MTA), a methyltransferase-selective inhibitor, followed by washing, a 5-day resting period, and restimulation with CpG (Figure 2D), as described.[29] Pretreatment of BMDMs with HK-EF increased TNF and IL-6 production upon rechallenge with CpG, an effect that was abolished upon MTA pretreatment (Figures 2E and S3A). Compared with unstimulated BMDMs, BMDMs stimulated with HK-EF for 24 h showed increased basal extracellular acidification rate (ECAR), indicative of glycolytic activity, a hallmark of TI[3,27] (Figures S3B and S3C), without an effect on basal oxygen consumption rate (Figure S3D). Preincubation with 2-deoxy-glucose (2-DG), a glycolysis inhibitor, effectively abolished the enhanced TNF production induced by HK-EF pretreatment of BMDMs (Figure 2F). TI induction by HK-EF was also found, to a similar extent as β-glucan-induced training,[30] in human peripheral blood mononuclear cells (PBMCs) from healthy donors (Figures 2G, 2H, and S3E). In conclusion, culturable *E. faecalis* was confirmed to translocate to the BM, and HK-EF induces TI in mouse and human myeloid cells.

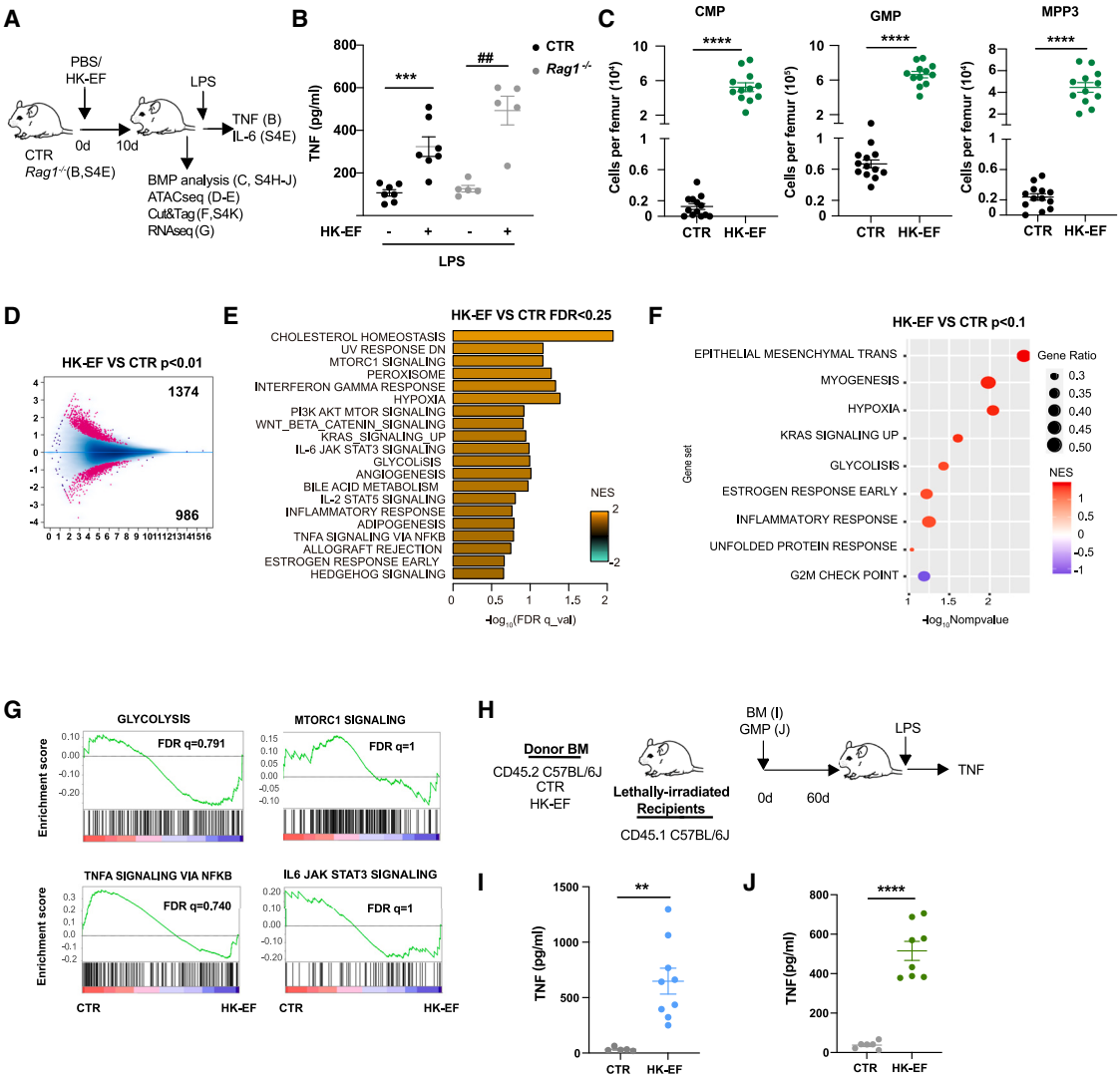

Figure 3. Systemic administration of HK-EF trains myeloid progenitors

(A and B) (A) Wild-type (WT) or *Rag1*$^{-/-}$ mice were treated or not with HK *E. faecalis* (HK-EF) i.v. followed by the indicated analyses 10 days later. (B) TNF concentration measured by ELISA in plasma obtained 1 h after LPS stimulation in the indicated genotypes and treatments. Two pooled independent experiments (n = 5–7).

(C) Graphs show total cell numbers per femur of common myeloid progenitors (CMPs), granulocyte-monocyte progenitors (GMPs), and multipotent progenitor cells (MPP3) at day 10 of protocol shown in (A). Three pooled independent experiments (n = 12–13).

(D and E) ATAC-seq analysis in GMPs sorted from BM at day 10 of protocol shown in (A). (D) MAplot showing 2.360 differentially accessible peaks between HK-EF and control (CTR) mice GMPs, with $p < 0.01$. (E) Bar plot showing enriched gene sets from the MSigDB Hallmark collection with FDR < 0.25. Positive normalized enrichment score (NES) values (orange color) and negative (green color) indicate congruent over- or under-expression of a pathway or function-associated genes in HK-EF compared with CTR. Only the top 20 hits (according to FDR) are represented. A pool of 3 mice was used per biological replicate, and 3 biological replicates were used per condition.

(F) H3K4me3 Cut&Tag analysis in GMPs at day 10 of protocol shown in (A). Bubble plot showing gene set enrichment analysis (GSEA) from the MSigDB Hallmark collection with an $p < 0.1$. Positive NES values (depicted in red) and negative (depicted in purple) indicate congruent over- or under-expression of a pathway or function-associated genes in HK-EF compared with CTR. Only the top 20 hits (according to FDR) are represented. Each biological replicate consisted of a pool of 3 mice, and 3 biological replicates were used per condition.

(G) RNA-seq analysis was performed on GMPs at day 10 of protocol shown in (A). GSEA for GMPs obtained from WT mice treated or not with HK-EF. GSEA profile from gene expression changes in glycolysis, mTOR, IL-6, and TNFA is highlighted.

(H–J) Donor mice were treated or not with HK-EF and rested for 10 days as in (A) and BM (I) or GMPs sorted from BM (J) were grafted to lethally irradiated CD45.1 C57BL/6J recipient mice. After 60 days, mice were challenged with LPS and TNF concentration measured by ELISA in plasma obtained 1 h after LPS stimulation.

(I) One representative experiment of two performed (n = 5–9). (J) Two pooled independent experiments (n = 6–8).

(B, C, I, and J) Individual data and mean ± SEM are shown. Unpaired Student's t test was used to compare groups. $^{**}p < 0.01$; $^{***}p < 0.005$; $^{****}p < 0.001$; $^{\#\#}p < 0.01$ vs. *Rag1*$^{-/-}$.

See also Figure S4.

Systemic administration of HK-EF trains myeloid progenitors

We then evaluated the ability of HK-EF to induce TI *in vivo* in the absence of intestinal barrier disruption. C57BL/6 mice were injected intravenously (i.v.) with live-EF or HK-EF, to test their ability to reach the BM. Both live-EF and HK-EF reached the BM within 2 h post injection but were not detected after 24 h (Figures S4A and S4B), suggesting a fast removal. Dose-response experiments showed that TI induction by HK-EF was bell shaped, persisted for at least 8 weeks (Figures S4C and S4D), and was independent of mature B and T cells (*Rag1*$^{-/-}$ mice, Figures 3A, 3B, and S4E). Indeed, several myeloid cell subsets contributed to this increased TNF production (Figure S4F). Consistent with our *in vitro* findings, TNF production was dampened when mice were treated with MTA in the drinking water (Figure S4G).

HK-EF administration resulted in BMP expansion (Figures 3A, 3C, and S4H–S4J). To determine whether this was due to an intrinsic change in epigenetic reprogramming or in transcriptional activity, we sorted GMPs from HK-EF-treated or control mice and performed ATAC-seq, H3K4me3 Cut&Tag, and RNA-seq. Our ATAC-seq results revealed differentially accessible peaks in GMPs from HK-EF-treated mice compared with control mice (Figure 3D). By ascribing open regions to gene promoters, GSEA showed an enrichment in pathways related to inflammation status, such as proinflammatory cytokines, mTOR, and pathways related to glycolysis in HK-EF mice, consistent with ATAC-seq (Figure 3E). H3K4me3 analysis by Cut&Tag also revealed more H3K4me3 peaks in HK-EF-treated mice compared with untreated mice (Figures 3F and S4K). Conversely, RNA-seq did not indicate transcriptional activity within the open chromatin regions related to inflammatory genes (Figure 3G). Given these epigenetic changes in BMPs, we next tested whether the TI phenotype was transferable by BM graft. After 60 days, mice grafted with BM from donors primed with HK-EF showed enhanced secondary response upon LPS rechallenge compared with mice grafted with BM from untreated mice (Figures 3H and 3I). Using GMPs instead of full BM also transferred the trained phenotype (Figures 3H and 3J). In conclusion, i.v. administration of HK-EF induces long-term TI associated with epigenetic changes in GMPs that can be transferred by BM graft.

HK-EF triggers Mincle-dependent TI in BMDMs

To explore the potential myeloid sensing receptor(s) for HK-EF, we analyzed the effect of inhibitors related to the CLR signaling pathway in HK-EF-induced TI. BMDMs from wild-type (WT) mice were pretreated with reversible inhibitors for 1 h prior to treatment with HK-EF, washed 1 day later to remove HK-EF and inhibitors. 5 days later, TNF and IL-6 production was evaluated upon restimulation with CpG (Figure 4A). Inhibition of Syk (Figures 4B and S5A), CARD9 (Figures 4C and S5B), or mTOR (Figures 4D and S5C) abolished the enhanced secondary response. Because several CLRs are upstream of this signaling pathway,[14] we used a reporter system consisting of B3Z cells expressing the extracellular domains of either Dectin-1, Dectin-2, or Mincle coupled to an intracellular CD3ζ domain to activate a nuclear factor of activated T cells (NFAT) reporter.[31,32] Although the reporter signal was triggered by specific ligands for every receptor, used as positive controls, only the Mincle reporter was activated by HK-EF (Figure 4E). Moreover, HK-EF also triggered the natural Mincle/Syk pathway in a B3Z cell line transfected with the WT Mincle receptors, FcRγ and Syk[32] (Figure 4F). To further validate this result, we stained HK-EF with Mincle-ectodomain-human-Fc chimera (Mincle-hFc), which bound specifically to a fraction of the bacteria exposing the ligand compared with the control human-Fc chimera (Figure 4G). In addition, BMDMs treated with HK-EF showed increased S6 ribosomal protein phosphorylation (pS6), indicative of mTOR activation. This was dependent on Mincle, as phosphorylation was abolished in BMDMs from *Clec4e*$^{-/-}$ mice (Figure 4H). To test the role of Mincle in the induction of TI by HK-EF, we generated BMDMs from WT and *Clec4e*$^{-/-}$ mice. Following treatment with HK-EF, BMDMs from *Clec4e*$^{-/-}$ mice lost the enhanced TNF production upon restimulation with CpG, LPS, or P3C4 observed in WT mice (Figures 4I, S5D, and S5E). Therefore, we conclude that HK-EF signals through the Mincle-Syk pathway, resulting in mTOR activation, a signaling pathway linked to increased TI.[27]

Mincle receptor stimulation induces TI

To further investigate the connection between Mincle and TI, we explored whether a known Mincle agonist, trehalose-6,6-dibehenate (TDB),[33] could also induce TI. Following treatment with TDB for 24 h, BMDMs were washed, rested for 5 days, and then re-challenged with CpG (Figure 5A). Pretreatment with the Mincle agonist enhanced TNF and IL-6 secretion by BMDMs upon CpG restimulation, an effect prevented by adding the epigenetic inhibitor MTA during TDB pretreatment (Figure 5B). The enhanced secondary response was abolished in *Clec4e*$^{-/-}$ BMDMs (Figure 5C). Moreover, 24 h of TDB stimulation increased basal glycolysis in BMDMs (Figure 5D) and increased pS6 in a Mincle-dependent fashion (Figure 5E), further validating the role of the Mincle receptor in the activation of the mTOR pathway. Other Mincle ligands, such as $GlcC_{14}C_{18}$ and $ManC_{14}C_{18}$,[34] and mucus from *Lactobacillus plantarum*-monocolonized mice[16] also induced TI *in vitro* to a similar extent as live or HK *E. faecalis*. In contrast, other abundant microbiota species that do not bind Mincle, such as *Escherichia coli*, did not induce TI *in vitro* (Figure 5F).

DSS treatment promotes the translocation of *Staphylococcus aureus* (Figure 2A), a microbiota species that contains ligands for Mincle, to the BM.[33] Indeed, we validated that *S. aureus* binds the Mincle-CD3ζ chimera and also signals through the WT Mincle receptor (Figure 5G). Pretreatment of BMDMs with HK-*S. aureus* (HK-SA) enhanced TNF production in the typical TI setting, an effect that was abolished in *Clec4e*$^{-/-}$ BMDMs (Figure 5H).

To analyze the ability of TDB to induce TI *in vivo* through Mincle, WT and *Clec4e*$^{-/-}$ mice were i.v. injected with dimethyl dioctadecyl ammonium bromide (DDA) liposomes containing or not containing TDB (DDA vs. DDA:TDB). Mice were re-challenged i.p. with LPS 10 days later as a readout for TI induction (Figure 5I). WT mice pretreated with DDA:TDB showed increased production of TNF compared with DDA, which was prevented in *Clec4e*$^{-/-}$ mice (Figure 5J). Collectively, these results demonstrate that Mincle activation induces TI hallmarks.

HK-EF induces Mincle-dependent TI *in vivo* that is protective against infection

To address the role of the Mincle receptor in HK-EF-mediated TI *in vivo*, WT and *Clec4e*$^{-/-}$ mice were primed with HK-EF and

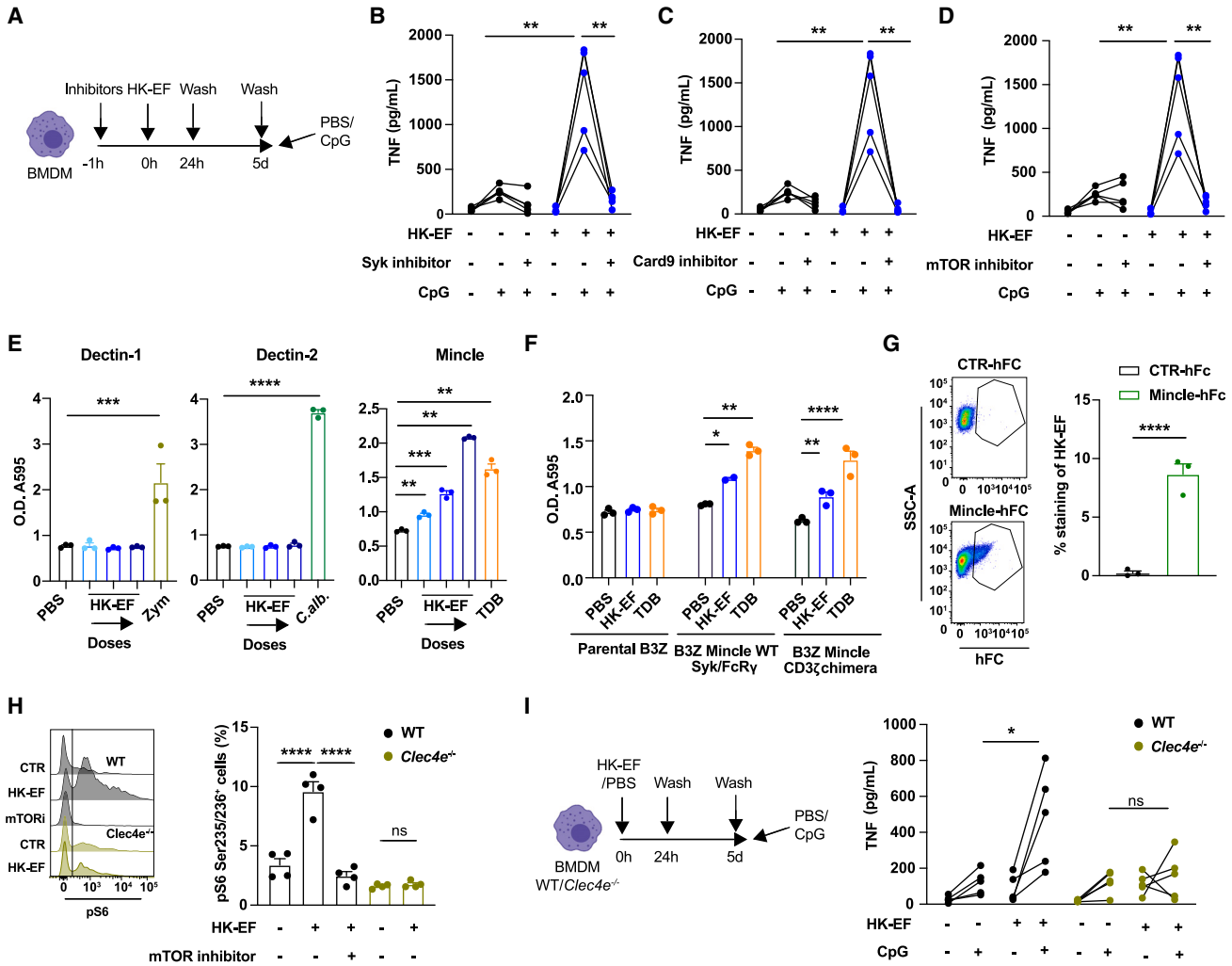

Figure 4. HK-EF triggers Mincle-dependent trained immunity in BMDMs

(A–D) (A) BMDMs were treated or not with HK-EF upon pretreatment with Syk inhibitor (B), Card9 inhibitor (C), or mTOR inhibitor (D), stimulated with CpG 5 days later, and TNF production measured by ELISA in culture supernatant of BMDMs 24 h after CpG stimulation. Paired Student's t test comparing independent BMDMs cultures ($n = 5$).

(E) NFAT reporter activity of B3Z cells expressing the extracellular domains of either mouse Dectin-1 (left), Dectin-2 (middle), or Mincle (right) coupled to an intracellular CD3ζ in response to the indicated stimuli: PBS, HK-EF, Zymosan (Zym), *Candida albicans* (*C. alb*), and trehalose-6,6-dibehenate (TDB). Increasing doses of HK-EF correspond to 2×10^5, 2×10^7, and 2×10^9 CFU per well. One representative experiment of three performed is shown. Statistical analysis was performed using one-way ANOVA with Bonferroni post hoc test.

(F) NFAT reporter activity in response to TDB or HK-EF (2×10^2 CFU) in B3Z cells parental, stably transfected with WT Mincle, Syk, and FcRγ, or B3Z expressing human Mincle-CD3ζ chimera. One representative experiment of three performed is shown. Statistical analysis was performed by one-way ANOVA with Bonferroni post hoc test.

(G) Representative plots (left) and graph depicting the frequency (right) of HK-EF stained with control-hFc or Mincle-hFc. Pool of three independent experiments.

(H) Representative histograms (left) and frequency of BMDMs from WT and *Clec4e*$^{-/-}$ mice showing high phosphorylation of S6 ribosomal protein (Ser235/236) measured by flow cytometry. Pool of two independent experiments. (G and H) Individual data and mean ± SEM.

(I) BMDMs from WT or *Clec4e*$^{-/-}$ mice were treated with PBS or HK-EF as indicated in the outline. TNF production measured by ELISA in culture supernatant of BMDMs from indicated treatments and stimulations. Paired Student's t test compares 5 independent WT and *Clec4e*$^{-/-}$ BMDMs cultures. *$p < 0.05$; **$p < 0.01$; ***$p < 0.005$; ****$p < 0.001$.

See also Figure S5.

10 days later challenged with LPS (Figure 6A). WT mice pretreated with HK-EF exhibited an enhanced TNF and IL-6 production following LPS rechallenge that was fully abolished in *Clec4e*$^{-/-}$ mice (Figures 6B and S6A). Moreover, HK-EF treatment resulted in a Mincle-dependent expansion of BMPs (Figures S6B and S6C). To determine whether epigenetic reprogramming induced by HK-EF depended on Mincle, we performed ATAC-seq and Cut&Tag on GMPs from WT or *Clec4e*$^{-/-}$ mice treated or not with HK-EF. GSEA of genes associated to open regions showed that the enrichment of pathways linked to inflammation in GMPs following treatment with HK-EF *in vivo* was largely prevented in *Clec4e*$^{-/-}$ mice (Figure 6C). The

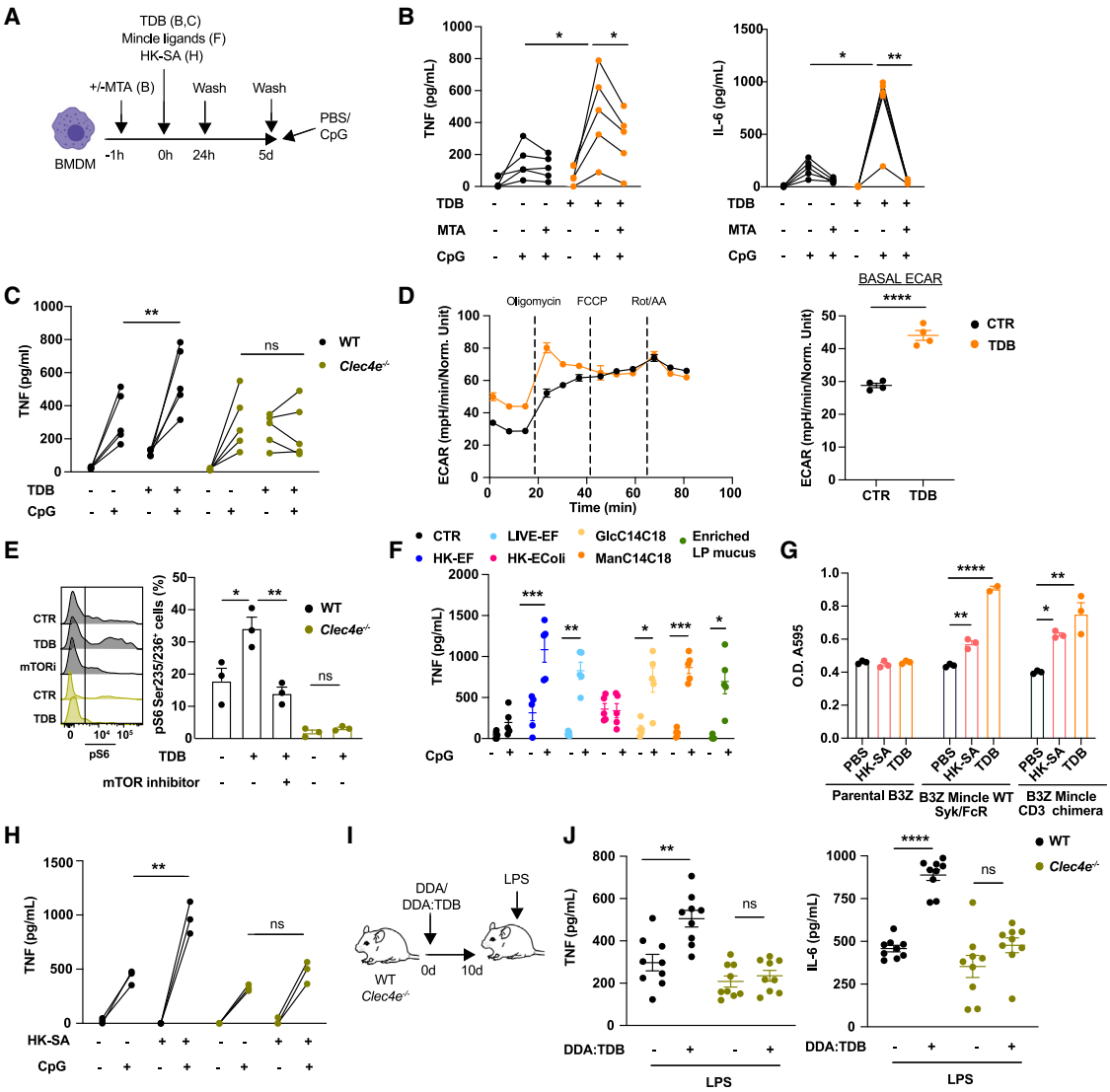

Figure 5. Mincle receptor stimulation induces trained immunity

(A and B) (A) BMDMs were treated or not with MTA 1 h before plating in trehalose-6,6-dibehenate (TDB)-coated wells. After 24 h, cells were re-plated in non-TDB-coated plates and rested for 5 days before stimulation with CpG for 24 h. (B) TNF (left) and IL-6 (right) production measured by ELISA in culture supernatant of BMDMs from indicated treatments and stimulations. Paired Student's t test compares 5 independent cultures.

(C) BMDMs from WT or *Clec4e*$^{-/-}$ mice were trained with TDB as described in (A). TNF production measured by ELISA in culture supernatant of BMDMs from indicated treatments and stimulations. Paired Student's t test compares 5 independent WT and *Clec4e*$^{-/-}$ BMDMs cultures.

(D) Time course kinetics extracellular acidification rate (ECAR) (left) and basal ECAR (right) of BMDMs stimulated or not with TDB for 24 h, measured in the MitoStress test in a Seahorse assay (n = 4).

(E) Representative histograms (left) and frequency of BMDMs from WT and *Clec4e*$^{-/-}$ mice stimulated or not for 24 h with TDB showing high phosphorylation of S6 ribosomal protein (Ser235/236) measured by flow cytometry. Pool of 3 independent experiments.

(F) BMDMs from WT mice were treated as in (A) but using as training stimuli HK or live EF, HK *E. coli* or some well-stablished ligands for Mincle, including $GclC_{14}C_{18}$, $ManC_{14}C_{18}$, and mucus from *Lactobacillus plantarum*-gavaged mice (enriched LP mucus). TNF production measured by ELISA in the culture supernatant of BMDMs from indicated treatments and stimulations. Paired Student's t test compares 5 independent WT BMDMs cultures.

(G) NFAT reporter activity in response to TDB or 2 × 10^2 CFU of HK *Staphylococcus aureus* (HK-SA) in B3Z cells parental, stably transfected with WT Mincle, Syk, and FcRγ or B3Z expressing human Mincle-CD3ζ chimera. One representative experiment of three performed is shown. One-way ANOVA with Bonferroni post hoc test.

(H) BMDMs from WT or *Clec4e*$^{-/-}$ mice were trained or not as indicated in (A) with HK-SA. TNF production was measured by ELISA in the culture supernatant of BMDMs from the indicated treatments and stimulations. Paired Student's t test compares 3 independent WT and *Clec4e*$^{-/-}$ BMDMs cultures.

(I and J) (I) WT or *Clec4e*$^{-/-}$ mice were treated with DDA or DDA:TDB i.v. and restimulated with LPS 10 days later. (J) TNF (left) and IL-6 (right) concentration measured by ELISA in plasma obtained 1 h after LPS stimulation. Three pooled independent experiments (n = 9).

Individual data and mean ± SEM are shown. Unpaired Student's t test. *p < 0.05; **p < 0.01; ***p < 0.005; ****p < 0.001.

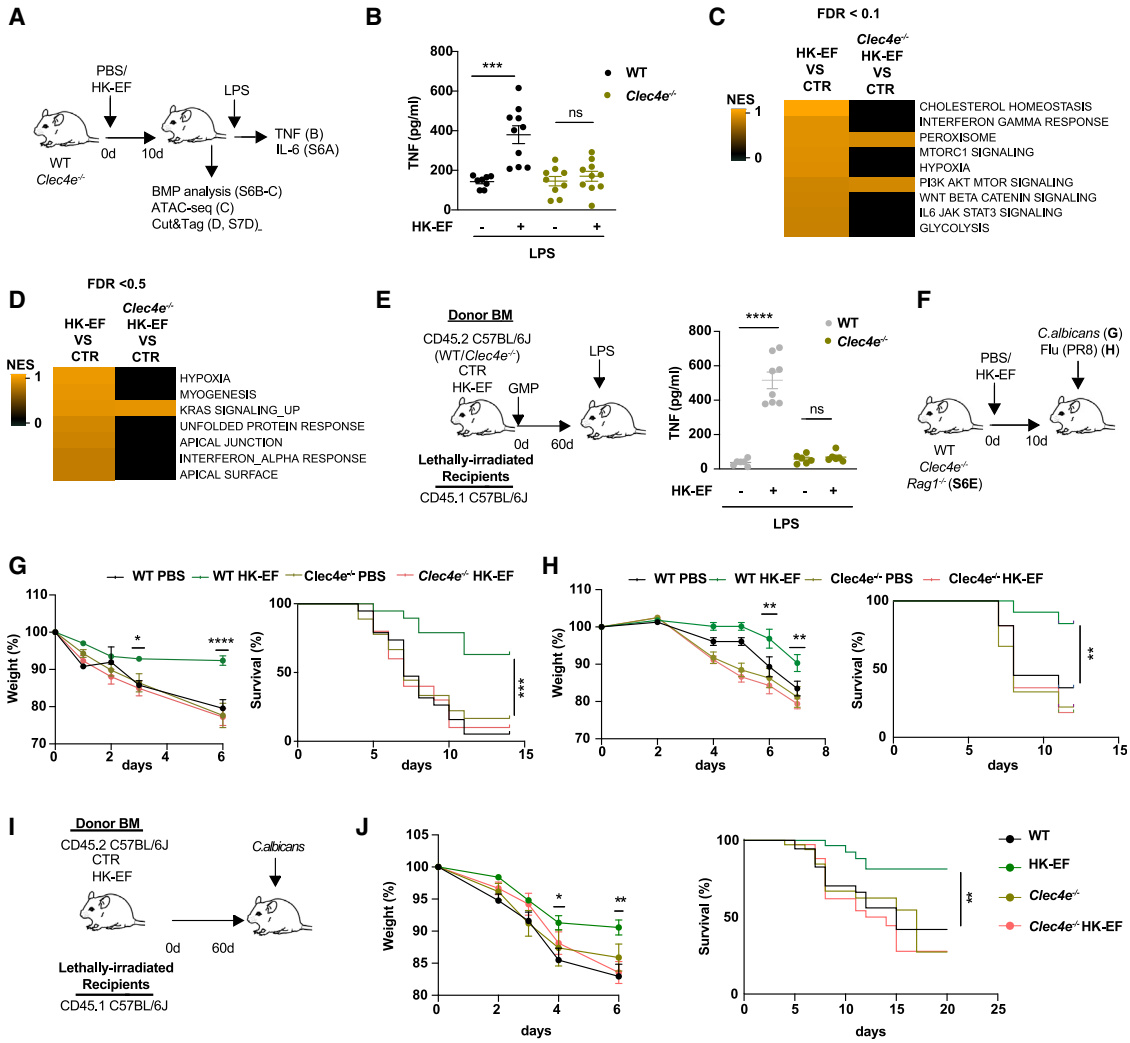

Figure 6. HK-EF induces Mincle-dependent trained immunity *in vivo* that is protective against infection

(A and B) (A) WT and *Clec4e*$^{-/-}$ mice were treated or not with HK-EF i.v. and challenged with LPS i.p. at day 10. (B) TNF concentration in plasma from mice of the indicated treatments and genotypes. Three pooled independent experiments (n = 8–10).

(C and D) Mice were either trained with HK-EF or left untreated and GMPs were sorted from BM at day 10 of protocol shown in (A) and analyzed by ATAC-seq (C) and H3K4me3 Cut&Tag analysis (D). Comparative heatmap representing normalized enrichment score (NES) values for gene sets from the MSigDB Hallmark collection, calculated through GSEA, after ascribing open regions to gene promoters. Gene sets have been selected among those enriched with FDR < 0.1 (C) or FDR < 0.5 (D). Positive and negative NES values indicate increased accessibility for gene-associated regions in mice treated with HK-EF or not (CTR), in WT or *Clec4e*$^{-/-}$ backgrounds, as indicated. A pool of 3 mice was used per biological replicate, and 3 biological replicates were used per condition.

(E) Donor mice were either treated with HK-EF or left untreated, followed by a 10-day resting period as outlined in (A). GMPs from these mice were subsequently grafted to lethally irradiated CD45.1 C57BL/6J recipient mice. After 60 days, the recipient mice were challenged with LPS. TNF concentration measured by ELISA in plasma obtained 1 h after LPS stimulation was measured by ELISA. One representative experiment out of two performed is shown (n = 5–9). WT mice are the same as in Figure 3I and shown here for comparison with *Clec4e*$^{-/-}$ mice tested in the same experiment.

(F–H) WT and *Clec4e*$^{-/-}$ mice treated or not with HK-EF were challenged with 1.5 × 10^5 CFU per mouse *C. albicans* i.v. (G) or 15 plaque-forming unit (PFU) per mouse of influenza A virus i.n. (H) at day 10. Weight loss (left) and survival curves (right) are shown.

(I and J) Donor mice were treated or not with HK-EF, followed by a 10-day resting period as in (A) and their BM used to graft lethally irradiated CD45.1 C57BL/6J recipient mice. After 60 days, mice were challenged with *C. albicans* 1.5 × 10^5 CFU per mouse i.v.

(J) Weight loss (left) and survival curves (right) are shown.

(B and E) Individual data and mean ± SEM are shown. Unpaired Student's t test was used to compare conditions. ***p < 0.005; ****p < 0.001.

(G, H, and J) Results from a pool of two independent experiments (n = 10). Two-way ANOVA test comparing CTR vs. HK-EF weight. Log rank (Mantel-Cox) test for survival curve comparison. *p < 0.05; **p < 0.01; ***p < 0.005; ****p < 0.001.

See also Figure S6.

increased number of H3K4me3-marked genes in mice treated with HK-EF *in vivo* compared with untreated mice was partially dependent on Mincle (Figure S6D). GSEA in the H3K4me3 differential peaks showed an enrichment in inflammatory and metabolic pathways similar to the ones shown by ATAC-seq (Figure 6D), indicating a Mincle-dependent HK-EF-induced epigenetic reprogramming in promoter gene regions. To explore whether this TI phenotype could be transferred, we grafted lethally irradiated mice with GMP from WT or *Clec4e*$^{-/-}$ donors primed or not with HK-EF. LPS rechallenge in the recipient mice 60 days after BM graft showed enhanced response in mice grafted with BM from HK-EF-primed donors in a Mincle-dependent manner (Figure 6E).

Next, we explored the potential for HK-EF-induced TI to protect against heterologous infection, a key hallmark of TI. WT and *Clec4e*$^{-/-}$ mice were i.v. trained or not with HK-EF and, 10 days later, mice were infected i.v. with a lethal dose of *Candida albicans* or influenza A virus (Figure 6F). Training with HK-EF resulted in reduced weight loss and improved survival to both pathogens compared with non-trained mice, which was Mincle dependent (Figures 6G and 6H). *Rag1*$^{-/-}$ mice showed that this protective effect was independent of T and B cells (Figure S6E). Consistently, Mincle-dependent HK-EF training also contributed to enhanced phagocytic capacity of trained BMDMs against *C. albicans* (Figure S6F). Mice grafted with BM from donors primed with HK-EF also showed antifungal protection in a Mincle-dependent manner (Figures 6I and 6J). Moreover, we tested whether intranasal (i.n.) administration of HK-EF, similar to other bacteria-based preparations that induce TI, such as MV130 and MV140,[3,35,36] could be protective against infection. WT mice were treated with HK-EF i.n., three times per week for 2 consecutive weeks, as described previously for i.n. polybacterial vaccines[3,36] (Figure S6G). 7 days after the last dose, mice were i.v. infected with a lethal dose of *C. albicans*. We found that i.n. HK-EF pretreatment resulted in reduced mortality compared with that in untreated mice (Figure S6H). Therefore, HK-EF induces TI *in vivo* via Mincle, resulting in protective immunity against heterologous infections, regardless of the administration route.

Mincle deficiency prevents TI and attenuates pathology associated with DSS-induced gut barrier disruption

We wondered whether TI induced by gut bacterial translocation would also depend on Mincle expression. Following DSS treatment to increase gut permeability in WT and *Clec4e*$^{-/-}$ mice, we generated BMDMs and treated them with LPS, CpG, or P3C4 (Figure 7A). In agreement with our results above (Figure 1B), this stimulation resulted in boosted TNF and IL-6 production in BMDMs obtained from DSS compared with that in untreated mice, a boosting effect that was dependent on Mincle (Figures 7B and S7A). Moreover, the expansion of BMPs upon DSS treatment was prevented in *Clec4e*$^{-/-}$ mice (Figures S7B and S7C).

To determine whether DSS-induced changes in epigenetic reprogramming were dependent on Mincle, we sorted GMPs from WT or *Clec4e*$^{-/-}$ mice treated or not with DSS, as indicated (Figure 7A), and performed ATAC-seq and Cut&Tag. GSEA of genes associated to open regions by ATAC-seq revealed an enrichment in pathways associated with inflammatory processes, which was prevented in DSS *Clec4e*$^{-/-}$ mice (Figure 7C). The number of genes marked with H3K4me3 in DSS WT mice compared with DSS *Clec4e*$^{-/-}$ mice was similar (Figure S7D). GSEA in the H3K4me3 differential peaks demonstrated enrichment in similar pathways as identified by ATAC-seq analysis in a largely Mincle-dependent manner (Figure 7D), indicating Mincle-dependent, DSS-induced epigenetic reprogramming in promoter gene regions. DSS treatment *in vivo* also enhanced the ability of BMDMs to phagocytose *C. albicans* in a Mincle-dependent manner (Figure S7E). This protection was also transferrable, as mice receiving BM grafts from DSS WT donors showed superior anti-fungal protection, in a Mincle-dependent manner, compared with those receiving BM from untreated mice (Figures 7E and 7F).

However, TI can also enhance detrimental inflammatory responses.[37] Because colitis is a pathological outcome of DSS treatment, we tested whether the absence of Mincle affected colitis development following a standard DSS-colitis protocol[38] (Figure 7G). *Clec4e*$^{-/-}$ mice showed reduced disease activity index, weight loss, and colon inflammation upon DSS-induced colitis compared with WT littermates (Figures 7H–7J). To confirm the key role of Mincle expression in BMPs for these effects, BM from WT or *Clec4e*$^{-/-}$ CD45.2^{+} donor mice was grafted into lethally irradiated recipient CD45.1^{+} mice. After 60 days, recipient mice were exposed to DSS (Figure S7F). BMDMs from these grafted mice kept the Mincle-dependent TI, similar to the donor BM (Figure S7G). Similarly, BMPs were expanded upon DSS treatment in a Mincle-dependent manner (Figure S7H). Correlating with the reduced TI phenotype in the BM, Mincle-deficient BM-derived cells led to an attenuated disease activity index, weight loss, and colon inflammation upon DSS-induced colitis compared with WT BM engraftment (Figures S7I–S7K). These results show that Mincle in BM-derived cells favors TI induced by bacterial translocation, along with the development of DSS colitis.

DISCUSSION

The potential mechanisms connecting gut microbial composition and/or impaired microbial containment remain unresolved.[1–3] Our results revealed that disruption of intestinal barrier integrity allows bacterial translocation to the BM, inducing TI characterized by epigenetic rewiring in GMPs, with a concomitant expansion of myeloid progenitor cells. The enhanced inflammatory response to secondary challenges was maintained in mice lacking B and T cells (*Rag1*$^{-/-}$ mice), pointing toward a phenotype driven by innate immune cells consistent with previous results in TI.[13] TI is a long-lasting process, intrinsic to BM cells, which are therefore transferable by BM graft.[12,39,40] Accordingly, we found that BMP cells grafted from DSS mice to healthy mice transfer a long-term trained phenotype, suggesting that the effect is independent of the primary stimulus (bacteria or gut damage), which is not carried over with the BM graft.

Although we identified several bacterial species able to reach BM in mice undergoing DSS treatment, *E. faecalis* was predominant in culture *ex vivo*. *E. faecalis* is an opportunistic bacteria, more abundant in the gut microbiota from inflammatory bowel disease (IBD) patients compared with healthy patients, but its potential role in IBD pathology remains unknown.[41] Translocation of *E. faecalis* is associated with gastric acid suppression in alcoholic liver disease, leading to liver inflammation and

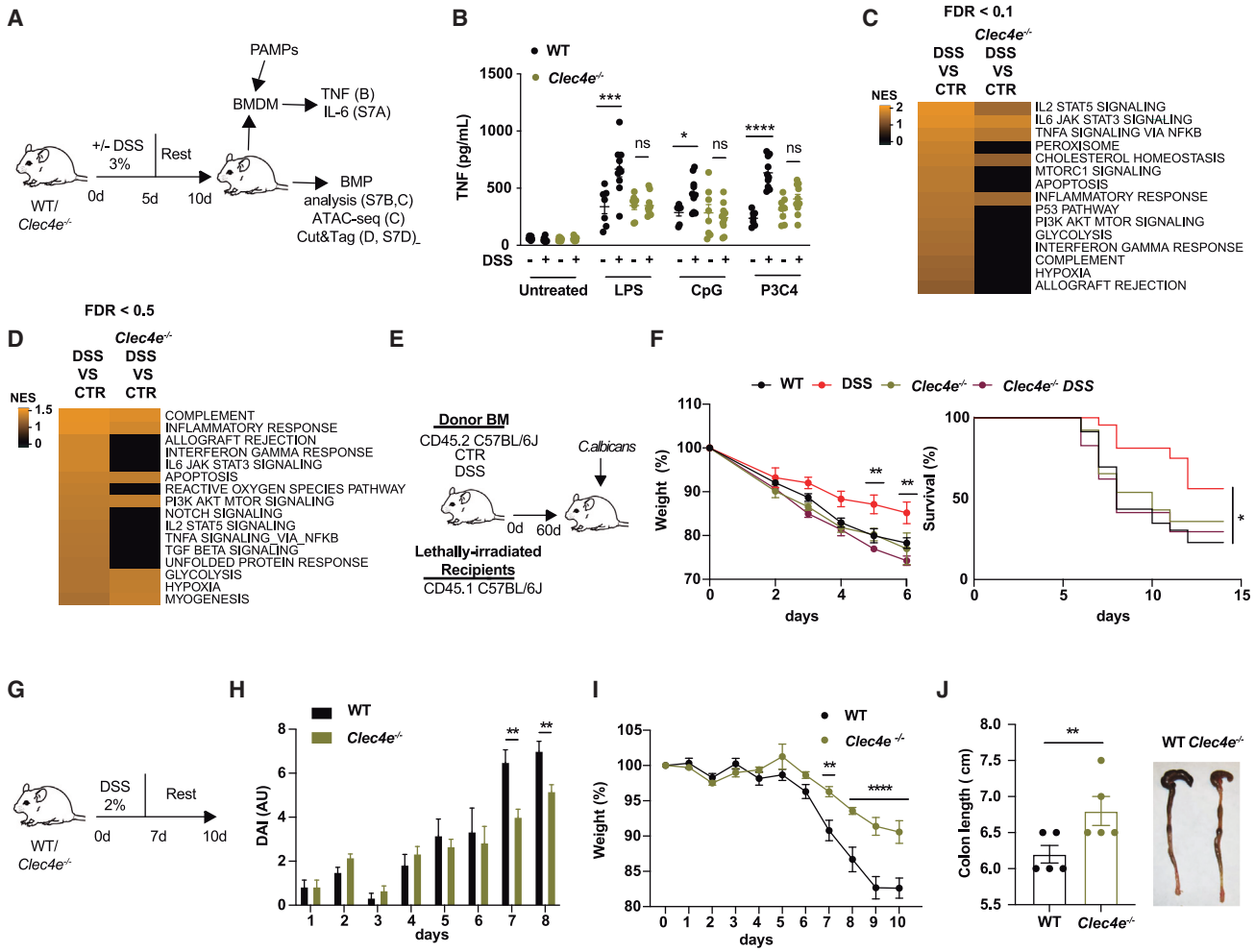

Figure 7. Mincle deficiency prevents trained immunity and attenuates pathology associated to DSS-induced gut barrier disruption

(A and B) (A) WT and *Clec4e*$^{-/-}$ mice were treated or not with DSS for 5 days and rested. At day 10, BM was extracted and BMDMs generated and stimulated with LPS, CpG, or P3C4 for 24 h. (B) TNF production measured by ELISA in culture supernatant of BMDMs from indicated treatments and stimulations. Two pooled independent experiments (n = 7–10).

(C and D) GMPs were sorted from BM at day 10 of protocol shown in (A) and analyzed by ATAC-seq (C) and H3K4me3 Cut&Tag (D). Comparative heatmap representing normalized enrichment score (NES) values for gene sets from the MSigDB Hallmark collection, as calculated by GSEA, after ascribing open regions to gene promoters. Gene sets have been selected among those enriched with FDR < 0.1 (C) or FDR < 0.5 (D). Positive and negative NES values indicate increased accessibility for gene-associated regions in mice treated with DSS or not (CTR), in WT or *Clec4e*$^{-/-}$ backgrounds, as indicated. A pool of 3 mice was used per biological replicate, and 3 biological replicates were used per condition.

(E and F) WT or *Clec4e*$^{-/-}$ donor mice were treated as in (A) and BM grafted into lethally irradiated CD45.1 C57BL/6J recipient mice. After 60 days, recipient mice were challenged with *C. albicans* 1.5 × 10^5 CFU per mouse i.v. (F) Weight loss (left) and survival curves (right) are shown. Results from a pool of two independent experiments (n = 10). Two-way ANOVA test comparing CTR vs. HK-EF weight. Log rank (Mantel-Cox) test for survival curve comparison.

(G–J) WT and *Clec4e*$^{-/-}$ mice were treated with DSS as indicated. (H) Disease activity index (DAI) (n = 8). Mean ± SEM. (I) Weight loss (n = 10). Mean ± SEM. (J) Colon length (n = 5). Individual data and mean ± SEM. Two pooled independent experiments. Unpaired Student's t test was used to compare groups. *p < 0.05; **p < 0.01; ***p < 0.005; ****p < 0.001.

See also Figure S7.

hepatocyte death.[42] Moreover, systemic translocation of other species of *Enterococcus*, such as *E. gallinarum*, triggers autoimmune responses in mice with genetic predisposition to lupus-like autoimmunity.[21] HK-EF was sufficient to prime hyperresponsiveness and metabolic reprogramming of myeloid cells, characterized by induction of glycolytic metabolism, as described for other TI inductors such as β-glucan,[29,30] BCG,[43] or MV130.[3] Besides, HK-EF trained human PBMCs as described for others TI-inducing stimuli, such as MV130[3] or β-glucan.[37,44] Systemic HK-EF induced TI *in vivo*, characterized by an expansion in myeloid progenitor cells, epigenetic changes in GMP, and enhanced response upon restimulation, which was independent of an adaptive immune response. This TI phenotype was transferred by GMP graft, with enhanced secondary responses detected up to 60 days after the graft, consistent with previous results on BM transfer of the TI phenotype.[12,39]

Our results unveiled that pathways downstream of Syk, via Card9 and also via mTOR, would contribute to the TI effect

produced by HK-EF. We identified Mincle as the upstream receptor coupled to this signaling pathway, specifically sensing *E. faecalis* and responsible for TI induction. Mincle is a well-characterized sensor for a diversity of microbial ligands that can mediate inflammatory responses.[33,45–47] Mincle can also detect microbiota signals and regulate intestinal immunity and mucosal barrier function.[16] Moreover, Mincle signaling promotes intestinal inflammation.[48] One of the main pathologies associated with bacterial translocation is IBD.[49,50] Biopsies from IBD patients, DSS-induced mouse colitis model, and 2,4,6-trinitrobenzene sulfonic acid-induced mouse colitis model show increased expression of Mincle, correlating with gut inflammation. Mincle deficiency attenuates experimental colitis, whereas administration of the Mincle agonist TDB exacerbates the disease.[48] Our results showing that microbial sensing by Mincle induced TI hallmarks and that both TI and DSS colitis are reduced in Mincle-deficient mice suggest the possibility that TI may contribute to gut inflammation.

On the bright side, TI is a potential immunotherapy to improve protection against heterologous infections.[36,39,51,52] We found that DSS treatment and HK-EF administration primed BMPs, generating a Mincle-dependent innate reprogramming that was protective against *C. albicans* and influenza A virus infection. This could imply a potential evolutionary advantage for selection of bacterial translocation in evolution. HK-EF conferred broad protection and was effective upon i.n. administration. This suggests that HK-EF could be used as a TI-based vaccine to prevent heterologous infections, similar to polybacterial preparations MV130[3,53,54] and MV140,[35,55] or BCG.[56]

Our findings suggest that gut microbiota translocation induces TI on BMPs, which can underlie pathologies related to low-grade systemic inflammation. The identification of *E. faecalis* translocation to the BM as a main driver of this effect and its sensing by the Mincle receptor in BMPs offers potential targets for intervention in pathophysiological settings where gut permeability is altered.

Limitations of the study

Our results have focused on the species that we could culture *ex vivo* from BM, *E. faecalis* and, to a lesser extent, *S. aureus*. However, 16S rRNA analysis suggests that other species are translocated and may contribute to this effect. TI induction upon DSS treatment is prevented in Mincle-deficient mice, suggesting that it is the key sensor of signals from microbiota translocation, but we cannot rule out that additional sensors for other bacterial products or metabolites from the translocated or even from the gut-resident microbiota also contribute to the epigenetic remodeling of BMPs. Although RNA-seq in parallel with ATAC-seq and CUT&Tag showed no transcriptional activation of inflammatory genes, additional approaches (e.g., H3K27ac epigenetics changes) were not tested. Epigenetic changes detected in H3K4me3-tagged regions in DSS and HK-EF compared with controls are involved in inflammatory responses. However, the overlap analysis between ATAC-seq and H3K4me3-tagged regions suggests that other important epigenetic changes induced by bacterial translocation occur in enhancer regions, which could have a relevant role in TI induced by bacterial translocation. Our results indicate that glycolysis is involved in the TI induced by HK-EF; however, future research would be necessary to understand the exact metabolic pathways underlying the potential regulation of TI induced by HK-EF. An additional limitation is the use of a very aggressive model of gut barrier disruption (DSS treatment) as a proof of principle for our study. Moreover, some experiments were performed at a time point in which gut healing after DSS is not complete, but we also performed experiments with longer resting periods, allowing for gut healing. In addition, the training phenotype was transferred upon BM graft to intact recipients, ruling out a direct role for gut damage or bacterial products. Future studies will dissect whether pathophysiological conditions that alter the gut barrier can trigger similar responses. Regarding the relevance in humans, although we have found that HK-EF trains human PBMCs *ex vivo*, whether a similar phenomenon is found in humans will require future studies of BMPs in patients with altered gut permeability.

RESOURCE AVAILABILITY

Lead contact

Requests for further information and resources should be directed to and will be fulfilled by the lead contact, David Sancho (dsancho@cnic.es).

Materials availability

This study did not generate new unique reagents.

Data and code availability

The data generated from RNA-seq, ATAC-seq, and Cut&Tag are available at Gene Expression Omnibus (GEO). GEO numbers and DOIs are listed in the key resources table. Any additional information required to reanalyze the data reported in this paper is available from the lead contact upon request.

ACKNOWLEDGMENTS

We are grateful to members of the D.S. laboratory for discussions and critical reading of the manuscript, particularly to Gillian Dunphy. We thank Jérôme Nigou for providing Mincle ligands and the CNIC facilities and personnel for assistance. I.R.-V. is funded by FJC2021-048099-I. M.M.-L. is supported by a Junior Leader postdoctoral fellowship from "la Caixa" Foundation (116923). A.R.-U. is supported by Community of Madrid (PIPF-2022/SAL-GL-2458). J.M. and C.G.-C. are predoctoral fellows of MINECO and Junta de Andalucía, respectively. C.d.F. is funded by Instituto de Salud Carlos III through the projects CP20/00106 and PI21-01178 (co-funded by European Union). J.D.'s laboratory is funded by Spanish Ministerio de Ciencia, Innovación y Universidades (MICIU) PID2020-116347RB-I00/AEI/10.13039/501100011033. Work in the D.S. laboratory is funded by the CNIC; by MICIU grants PID2022-137712OB-I00, CPP2021-008310, and CPP2022-009762 from the MICIU/AEI/10.13039/501100011033 Agencia Estatal de Investigación (AEI) and Unión Europea NextGenerationEU/PRTR; by the Comunidad de Madrid (P2022/BMD-7333 INMUNOVAR-CM); by the Scientific Foundation of the Spanish Association Against Cancer (AECC-PRYGN246642SANC); by Worldwide Cancer Research (WWCR-25-0080); by the European Union (ERC-2023-PoC); by a research agreement with Inmunotek S.L.; and by "la Caixa" Foundation (LCF/PR/HR23/52430012 and LCF/PR/HR22/52420019). The CNIC is supported by the Instituto de Salud Carlos III (ISCIII), the MICIU, and the Pro CNIC Foundation, and it is a Severo Ochoa Center of Excellence (CEX2020-001041-S, funded by MICIU/AEI/10.13039/501100011033). Work in the S.I. laboratory is funded by the MICIU, AEI, and FEDER through grants RTI2018-094484-B-I00, PID2021-125415OB-I00, and RYC-2016-19463.

AUTHOR CONTRIBUTIONS

I.R.-V. and D.S. conceived and designed the project and laboratory experiments. I.R.-V., P.B., A.J.-C., S.M.-C., M.R.-T., M.F.-M., A.R.-U., V.N., C.G.-C., P.M.-M., M.B.-G., C.M.D.-R., J.M., M.M.-L., and S.I. performed the laboratory experiments. I.R.-V., S.I., A.J.-C., and D.S. analyzed and interpreted the laboratory experiments. M.J.G., F.S.-C., A.Q., A.D., E.P., L.C., M.M.-L., C.d.F., and J.L.S. performed essential analyses. J.D. provided essential reagents. I.F.-L.

provided essential support. I.R.-V. and D.S. wrote the manuscript. All authors revised and edited the manuscript prior to submission.

DECLARATION OF INTERESTS

J.L.S., L.C., C.M.D.-R., S.I., and S.M.-C. were employees of Inmunotek S.L. or Fundación Inmunotek at the time of the work. The D.S. lab receives funds from a collaboration agreement between CNIC and Inmunotek.

STAR★METHODS

Detailed methods are provided in the online version of this paper and include the following:

- KEY RESOURCES TABLE
- EXPERIMENTAL MODEL AND STUDY PARTICIPANT DETAILS
  - Mice
  - Cell lines
  - Differentiation, culture, and stimulation of BMDMs
  - Human peripheral blood mononuclear cell isolation
- METHOD DETAILS
  - DSS models
  - Isolation and *ex vivo* stimulation of murine bone marrow cells
  - Trained immunity protocol *in vitro*
  - Trained immunity protocol *in vivo*
  - Flow cytometry analysis of bone marrow progenitors
  - mTOR activation by Phospho-S6 staining
  - Quantification of cytokines
  - Bone marrow graft
  - Analysis of bacterial translocation
  - Germ-free mice inoculation
  - Germ-free mice mono-colonization
  - Bacteria identification
  - *Enterococcus faecalis* culture
  - Flow cytometry analysis of Spleen
  - Seahorse assay
  - Fungal infections
  - Phagocytosis assay
  - Viral infection
  - B3Z reporter assays
  - Human Fc recombinant assay
  - ATAC-Sequencing
  - ATAC-Seq data analysis
  - Cut&Tag Sequencing
  - Cut&Tag data analysis
  - RNA-Seq sequencing
  - RNA-Seq analysis
  - DDA:TDB liposomes
- QUANTIFICATION AND STATISTICAL ANALYSIS

SUPPLEMENTAL INFORMATION

Supplemental information can be found online at https://doi.org/10.1016/j.immuni.2024.12.012.

Received: August 2, 2024
Revised: October 29, 2024
Accepted: December 31, 2024
Published: January 22, 2025

REFERENCES

1. Akdis, C.A. (2021). Does the epithelial barrier hypothesis explain the increase in allergy, autoimmunity and other chronic conditions? Nat. Rev. Immunol. *21*, 739–751. https://doi.org/10.1038/s41577-021-00538-7.
2. Tilg, H., Zmora, N., Adolph, T.E., and Elinav, E. (2020). The intestinal microbiota fuelling metabolic inflammation. Nat. Rev. Immunol. *20*, 40–54. https://doi.org/10.1038/s41577-019-0198-4.
3. Brandi, P., Conejero, L., Cueto, F.J., Martínez-Cano, S., Dunphy, G., Gómez, M.J., Relaño, C., Saz-Leal, P., Enamorado, M., Quintas, A., et al. (2022). Trained immunity induction by the inactivated mucosal vaccine MV130 protects against experimental viral respiratory infections. Cell Rep. *38*, 110184. https://doi.org/10.1016/j.celrep.2021.110184.
4. Vuscan, P., Kischkel, B., Joosten, L.A.B., and Netea, M.G. (2024). Trained immunity: general and emerging concepts. Immunol. Rev. *323*, 164–185. https://doi.org/10.1111/imr.13326.
5. Netea, M.G., Domínguez-Andrés, J., Barreiro, L.B., Chavakis, T., Divangahi, M., Fuchs, E., Joosten, L.A.B., van der Meer, J.W.M., Mhlanga, M.M., Mulder, W.J.M., et al. (2020). Defining trained immunity and its role in health and disease. Nat. Rev. Immunol. *20*, 375–388. https://doi.org/10.1038/s41577-020-0285-6.
6. Krautkramer, K.A., Kreznar, J.H., Romano, K.A., Vivas, E.I., Barrett-Wilt, G.A., Rabaglia, M.E., Keller, M.P., Attie, A.D., Rey, F.E., and Denu, J.M. (2016). Diet-Microbiota Interactions Mediate Global Epigenetic Programming in Multiple Host Tissues. Mol. Cell *64*, 982–992. https://doi.org/10.1016/j.molcel.2016.10.025.
7. Schulthess, J., Pandey, S., Capitani, M., Rue-Albrecht, K.C., Arnold, I., Franchini, F., Chomka, A., Ilott, N.E., Johnston, D.G.W., Pires, E., et al. (2019). The short chain fatty acid butyrate imprints an antimicrobial program in macrophages. Immunity *50*, 432–445.e7. https://doi.org/10.1016/j.immuni.2018.12.018.
8. Luo, Y., Chen, G.-L., Hannemann, N., Ipseiz, N., Krönke, G., Bäuerle, T., Munos, L., Wirtz, S., Schett, G., and Bozec, A. (2015). Microbiota from obese mice regulate hematopoietic stem cell differentiation by altering the bone niche. Cell Metab. *22*, 886–894. https://doi.org/10.1016/j.cmet.2015.08.020.
9. Clarke, T.B., Davis, K.M., Lysenko, E.S., Zhou, A.Y., Yu, Y., and Weiser, J.N. (2010). Recognition of peptidoglycan from the microbiota by Nod1 enhances systemic innate immunity. Nat. Med. *16*, 228–231. https://doi.org/10.1038/nm.2087.
10. Deshmukh, H.S., Liu, Y., Menkiti, O.R., Mei, J., Dai, N., O'Leary, C.E., Oliver, P.M., Kolls, J.K., Weiser, J.N., and Worthen, G.S. (2014). The microbiota regulates neutrophil homeostasis and host resistance to Escherichia coli K1 sepsis in neonatal mice. Nat. Med. *20*, 524–530. https://doi.org/10.1038/nm.3542.
11. Trompette, A., Gollwitzer, E.S., Yadava, K., Sichelstiel, A.K., Sprenger, N., Ngom-Bru, C., Blanchard, C., Junt, T., Nicod, L.P., Harris, N.L., et al. (2014). Gut microbiota metabolism of dietary fiber influences allergic airway disease and hematopoiesis. Nat. Med. *20*, 159–166. https://doi.org/10.1038/nm.3444.
12. Mitroulis, I., Ruppova, K., Wang, B., Chen, L.-S., Grzybek, M., Grinenko, T., Eugster, A., Troullinaki, M., Palladini, A., Kourtzelis, I., et al. (2018). Modulation of myelopoiesis progenitors is an integral component of trained immunity. Cell *172*, 147–161.e12. https://doi.org/10.1016/j.cell.2017.11.034.
13. Quintin, J., Saeed, S., Martens, J.H.A., Giamarellos-Bourboulis, E.J., Ifrim, D.C., Logie, C., Jacobs, L., Jansen, T., Kullberg, B.-J., Wijmenga, C., et al. (2012). Candida albicans infection affords protection against reinfection via functional reprogramming of monocytes. Cell Host Microbe *12*, 223–232. https://doi.org/10.1016/j.chom.2012.06.006.
14. Sancho, D., and Reis e Sousa, C. (2012). Signaling by myeloid C-type lectin receptors in immunity and homeostasis. Annu. Rev. Immunol. *30*, 491–529. https://doi.org/10.1146/annurev-immunol-031210-101352.
15. Miyake, Y., and Yamasaki, S. (2020). Immune recognition of pathogen-derived glycolipids through mincle. Adv. Exp. Med. Biol. *1204*, 31–56. https://doi.org/10.1007/978-981-15-1580-4_2.
16. Martínez-López, M., Iborra, S., Conde-Garrosa, R., Mastrangelo, A., Danne, C., Mann, E.R., Reid, D.M., Gaboriau-Routhiau, V., Chaparro, M., Lorenzo, M.P., et al. (2019). Microbiota sensing by Mincle-Syk axis in dendritic cells regulates interleukin-17 and -22 production and promotes intestinal barrier integrity. Immunity *50*, 446–461.e9. https://doi.org/10.1016/j.immuni.2018.12.020.

17. Costa, F.R.C., Françozo, M.C.S., de Oliveira, G.G., Ignacio, A., Castoldi, A., Zamboni, D.S., Ramos, S.G., Câmara, N.O., de Zoete, M.R., Palm, N.W., et al. (2016). Gut microbiota translocation to the pancreatic lymph nodes triggers NOD2 activation and contributes to T1D onset. J. Exp. Med. *213*, 1223–1239. https://doi.org/10.1084/jem.20150744.

18. Daillère, R., Vétizou, M., Waldschmitt, N., Yamazaki, T., Isnard, C., Poirier-Colame, V., Duong, C.P.M., Flament, C., Lepage, P., Roberti, M.P., et al. (2016). Enterococcus hirae and Barnesiella intestinihominis facilitate cyclophosphamide-induced therapeutic immunomodulatory effects. Immunity *45*, 931–943. https://doi.org/10.1016/j.immuni.2016.09.009.

19. Meisel, M., Hinterleitner, R., Pacis, A., Chen, L., Earley, Z.M., Mayassi, T., Pierre, J.F., Ernest, J.D., Galipeau, H.J., Thuille, N., et al. (2018). Microbial signals drive pre-leukaemic myeloproliferation in a Tet2-deficient host. Nature *557*, 580–584. https://doi.org/10.1038/s41586-018-0125-z.

20. Viaud, S., Saccheri, F., Mignot, G., Yamazaki, T., Daillère, R., Hannani, D., Enot, D.P., Pfirschke, C., Engblom, C., Pittet, M.J., et al. (2013). The intestinal microbiota modulates the anticancer immune effects of cyclophosphamide. Science *342*, 971–976. https://doi.org/10.1126/science.1240537.

21. Manfredo Vieira, S., Hiltensperger, M., Kumar, V., Zegarra-Ruiz, D., Dehner, C., Khan, N., Costa, F.R.C., Tiniakou, E., Greiling, T., Ruff, W., et al. (2018). Translocation of a gut pathobiont drives autoimmunity in mice and humans. Science *359*, 1156–1161. https://doi.org/10.1126/science.aar7201.

22. Macpherson, A.J., and Uhr, T. (2004). Induction of protective IgA by intestinal dendritic cells carrying commensal bacteria. Science *303*, 1662–1665. https://doi.org/10.1126/science.1091334.

23. Hand, T.W., Dos Santos, L.M., Bouladoux, N., Molloy, M.J., Pagán, A.J., Pepper, M., Maynard, C.L., Elson, C.O., 3rd, and Belkaid, Y. (2012). Acute gastrointestinal infection induces long-lived microbiota-specific T cell responses. Science *337*, 1553–1556. https://doi.org/10.1126/science.1220961.

24. Sandler, N.G., and Douek, D.C. (2012). Microbial translocation in HIV infection: causes, consequences and treatment opportunities. Nat. Rev. Microbiol. *10*, 655–666. https://doi.org/10.1038/nrmicro2848.

25. Jensen, S.K., Pærregaard, S.I., Brandum, E.P., Jørgensen, A.S., Hjortø, G.M., and Jensen, B.A.H. (2022). Rewiring host-microbe interactions and barrier function during gastrointestinal inflammation. Gastroenterol. Rep. *10*, goac008. https://doi.org/10.1093/gastro/goac008.

26. de la Visitación, N., Robles-Vera, I., Moleón, J., González-Correa, C., Aguilera-Sánchez, N., Toral, M., Gómez-Guzmán, M., Sánchez, M., Jiménez, R., Martin-Morales, N., et al. (2021). Gut microbiota has a crucial role in the development of hypertension and vascular dysfunction in toll-like receptor 7-driven lupus autoimmunity. Antioxidants (Basel, Switzerland) *10*, 1426. https://doi.org/10.3390/antiox10091426.

27. Cheng, S.-C., Quintin, J., Cramer, R.A., Shepardson, K.M., Saeed, S., Kumar, V., Giamarellos-Bourboulis, E.J., Martens, J.H.A., Rao, N.A., Aghajanirefah, A., et al. (2014). mTOR- and HIF-1α-mediated aerobic glycolysis as metabolic basis for trained immunity. Science *345*, 1250684. https://doi.org/10.1126/science.1250684.

28. Ha, C.W.Y., Martin, A., Sepich-Poore, G.D., Shi, B., Wang, Y., Gouin, K., Humphrey, G., Sanders, K., Ratnayake, Y., Chan, K.S.L., et al. (2020). Translocation of viable gut microbiota to mesenteric adipose drives formation of creeping fat in humans. Cell *183*, 666–683.e17. https://doi.org/10.1016/j.cell.2020.09.009.

29. Saz-Leal, P., Del Fresno, C., Brandi, P., Martínez-Cano, S., Dungan, O.M., Chisholm, J.D., Kerr, W.G., and Sancho, D. (2018). Targeting SHIP-1 in Myeloid Cells Enhances Trained Immunity and Boosts Response to Infection. Cell Rep. *25*, 1118–1126. https://doi.org/10.1016/j.celrep.2018.09.092.

30. Stothers, C.L., Burelbach, K.R., Owen, A.M., Patil, N.K., McBride, M.A., Bohannon, J.K., Luan, L., Hernandez, A., Patil, T.K., Williams, D.L., et al. (2021). β-Glucan Induces Distinct and Protective Innate Immune Memory in Differentiated Macrophages. J. Immunol. *207*, 2785–2798. https://doi.org/10.4049/jimmunol.2100107.

31. Sancho, D., Joffre, O.P., Keller, A.M., Rogers, N.C., Martínez, D., Hernanz-Falcón, P., Rosewell, I., and Reis e Sousa, C. (2009). Identification of a dendritic cell receptor that couples sensing of necrosis to immunity. Nature *458*, 899–903. https://doi.org/10.1038/nature07750.

32. Iborra, S., Martínez-López, M., Cueto, F.J., Conde-Garrosa, R., Del Fresno, C., Izquierdo, H.M., Abram, C.L., Mori, D., Campos-Martín, Y., Reguera, R.M., et al. (2016). Leishmania uses mincle to target an inhibitory ITAM signaling pathway in dendritic cells that dampens adaptive immunity to infection. Immunity *45*, 788–801. https://doi.org/10.1016/j.immuni.2016.09.012.

33. Schoenen, H., Bodendorfer, B., Hitchens, K., Manzanero, S., Werninghaus, K., Nimmerjahn, F., Agger, E.M., Stenger, S., Andersen, P., Ruland, J., et al. (2010). Cutting edge: Mincle is essential for recognition and adjuvanticity of the mycobacterial cord factor and its synthetic analog trehalose-dibehenate. J. Immunol. *184*, 2756–2760. https://doi.org/10.4049/jimmunol.0904013.

34. Decout, A., Silva-Gomes, S., Drocourt, D., Barbe, S., André, I., Cueto, F.J., Lioux, T., Sancho, D., Pérouzel, E., Vercellone, A., et al. (2017). Rational design of adjuvants targeting the C-type lectin Mincle. Proc. Natl. Acad. Sci. USA *114*, 2675–2680. https://doi.org/10.1073/pnas.1612421114.

35. Martin-Cruz, L., Sevilla-Ortega, C., Benito-Villalvilla, C., Diez-Rivero, C.M., Sanchez-Ramón, S., Subiza, J.L., and Palomares, O. (2020). A combination of polybacterial MV140 and Candida albicans V132 as a potential novel trained immunity-based vaccine for genitourinary tract infections. Front. Immunol. *11*, 612269. https://doi.org/10.3389/fimmu.2020.612269.

36. Del Fresno, C., García-Arriaza, J., Martínez-Cano, S., Heras-Murillo, I., Jarit-Cabanillas, A., Amores-Iniesta, J., Brandi, P., Dunphy, G., Suay-Corredera, C., Pricolo, M.R., et al. (2021). The bacterial mucosal immunotherapy MV130 protects against SARS-CoV-2 infection and improves COVID-19 vaccines immunogenicity. Front. Immunol. *12*, 748103. https://doi.org/10.3389/fimmu.2021.748103.

37. Bekkering, S., Domínguez-Andrés, J., Joosten, L.A.B., Riksen, N.P., and Netea, M.G. (2021). Trained immunity: reprogramming innate immunity in health and disease. Annu. Rev. Immunol. *39*, 667–693. https://doi.org/10.1146/annurev-immunol-102119-073855.

38. Wirtz, S., Neufert, C., Weigmann, B., and Neurath, M.F. (2007). Chemically induced mouse models of intestinal inflammation. Nat. Protoc. *2*, 541–546. https://doi.org/10.1038/nprot.2007.41.

39. Kaufmann, E., Sanz, J., Dunn, J.L., Khan, N., Mendonça, L.E., Pacis, A., Tzelepis, F., Pernet, E., Dumaine, A., Grenier, J.-C., et al. (2018). BCG educates hematopoietic stem cells to generate protective innate immunity against tuberculosis. Cell *172*, 176–190.e19. https://doi.org/10.1016/j.cell.2017.12.031.

40. Mitroulis, I., Kalafati, L., Hajishengallis, G., and Chavakis, T. (2018). Myelopoiesis in the context of innate immunity. J. Innate Immun. *10*, 365–372. https://doi.org/10.1159/000489406.

41. Roche-Lima, A., Carrasquillo-Carrión, K., Gómez-Moreno, R., Cruz, J.M., Velázquez-Morales, D.M., Rogozin, I.B., and Baerga-Ortiz, A. (2018). The Presence of genotoxic and/or Pro-inflammatory Bacterial Genes in Gut metagenomic Databases and Their Possible Link with inflammatory bowel Diseases. Front. Genet. *9*, 116. https://doi.org/10.3389/fgene.2018.00116.

42. Llorente, C., Jepsen, P., Inamine, T., Wang, L., Bluemel, S., Wang, H.J., Loomba, R., Bajaj, J.S., Schubert, M.L., Sikaroodi, M., et al. (2017). Gastric acid suppression promotes alcoholic liver disease by inducing overgrowth of intestinal Enterococcus. Nat. Commun. *8*, 837. https://doi.org/10.1038/s41467-017-00796-x.

43. Funes, S.C., Rios, M., Fernández-Fierro, A., Di Genaro, M.S., and Kalergis, A.M. (2022). Trained immunity contribution to autoimmune and inflammatory disorders. Front. Immunol. *13*, 868343. https://doi.org/10.3389/fimmu.2022.868343.

44. Hermans, L., De Pelsmaeker, S., Denaeghel, S., Cox, E., Favoreel, H.W., and Devriendt, B. (2021). β-Glucan-Induced IL-10 Secretion by monocytes Triggers Porcine NK Cell cytotoxicity. Front. Immunol. *12*, 634402. https://doi.org/10.3389/fimmu.2021.634402.

45. Ishikawa, E., Ishikawa, T., Morita, Y.S., Toyonaga, K., Yamada, H., Takeuchi, O., Kinoshita, T., Akira, S., Yoshikai, Y., and Yamasaki, S. (2009). Direct recognition of the mycobacterial glycolipid, trehalose dimycolate, by C-type lectin Mincle. J. Exp. Med. *206*, 2879–2888. https://doi.org/10.1084/jem.20091750.

46. Ishikawa, T., Itoh, F., Yoshida, S., Saijo, S., Matsuzawa, T., Gonoi, T., Saito, T., Okawa, Y., Shibata, N., Miyamoto, T., et al. (2013). Identification of distinct ligands for the C-type lectin receptors Mincle and Dectin-2 in the pathogenic fungus Malassezia. Cell Host Microbe *13*, 477–488. https://doi.org/10.1016/j.chom.2013.03.008.

47. Del Fresno, C., Iborra, S., Saz-Leal, P., Martínez-López, M., and Sancho, D. (2018). Flexible signaling of myeloid C-type lectin receptors in immunity and inflammation. Front. Immunol. *9*, 804. https://doi.org/10.3389/fimmu.2018.00804.

48. Gong, W., Zheng, T., Guo, K., Fang, M., Xie, H., Li, W., Tang, Q., Hong, Z., Ren, H., Gu, G., et al. (2020). Mincle/Syk signalling promotes intestinal mucosal inflammation through induction of macrophage pyroptosis in Crohn's disease. J. Crohns Colitis *14*, 1734–1747. https://doi.org/10.1093/ecco-jcc/jjaa088.

49. Sokol, H., Leducq, V., Aschard, H., Pham, H.-P., Jegou, S., Landman, C., Cohen, D., Liguori, G., Bourrier, A., Nion-Larmurier, I., et al. (2017). Fungal microbiota dysbiosis in IBD. Gut *66*, 1039–1048. https://doi.org/10.1136/gutjnl-2015-310746.

50. Ni, J., Wu, G.D., Albenberg, L., and Tomov, V.T. (2017). Gut microbiota and IBD: causation or correlation? Nat. Rev. Gastroenterol. Hepatol. *14*, 573–584. https://doi.org/10.1038/nrgastro.2017.88.

51. Arts, R.J.W., Moorlag, S.J.C.F.M., Novakovic, B., Li, Y., Wang, S.-Y., Oosting, M., Kumar, V., Xavier, R.J., Wijmenga, C., Joosten, L.A.B., et al. (2018). BCG vaccination protects against experimental viral infection in humans through the induction of cytokines associated with trained immunity. Cell Host Microbe *23*, 89–100.e5. https://doi.org/10.1016/j.chom.2017.12.010.

52. Ziogas, A., and Netea, M.G. (2022). Trained immunity-related vaccines: innate immune memory and heterologous protection against infections. Trends Mol. Med. *28*, 497–512. https://doi.org/10.1016/j.molmed.2022.03.009.

53. Vázquez, A., Fernández-Sevilla, L.M., Jiménez, E., Pérez-Cabrera, D., Yañez, R., Subiza, J.L., Varas, A., Valencia, J., and Vicente, A. (2020). Involvement of mesenchymal stem cells in oral mucosal bacterial immunotherapy. Front. Immunol. *11*, 567391. https://doi.org/10.3389/fimmu.2020.567391.

54. Sánchez-Ramón, S., Conejero, L., Netea, M.G., Sancho, D., Palomares, Ó., and Subiza, J.L. (2018). Trained immunity-based vaccines: A new paradigm for the development of broad-spectrum anti-infectious formulations. Front. Immunol. *9*, 2936. https://doi.org/10.3389/fimmu.2018.02936.

55. Martín-Cruz, L., Angelina, A., Baydemir, I., Bulut, Ö., Subiza, J.L., Netea, M.G., Domínguez-Andrés, J., and Palomares, O. (2022). Candida albicans V132 induces trained immunity and enhances the responses triggered by the polybacterial vaccine MV140 for genitourinary tract infections. Front. Immunol. *13*, 1066383. https://doi.org/10.3389/fimmu.2022.1066383.

56. Jeyanathan, M., Vaseghi-Shanjani, M., Afkhami, S., Grondin, J.A., Kang, A., D'Agostino, M.R., Yao, Y., Jain, S., Zganiacz, A., Kroezen, Z., et al. (2022). Parenteral BCG vaccine induces lung-resident memory macrophages and trained immunity via the gut-lung axis. Nat. Immunol. *23*, 1687–1702. https://doi.org/10.1038/s41590-022-01354-4.

57. Wells, C.A., Salvage-Jones, J.A., Li, X., Hitchens, K., Butcher, S., Murray, R.Z., Beckhouse, A.G., Lo, Y.-L.-S., Manzanero, S., Cobbold, C., et al. (2008). The macrophage-inducible C-type lectin, mincle, is an essential component of the innate immune response to Candida albicans. J. Immunol. *180*, 7404–7413. https://doi.org/10.4049/jimmunol.180.11.7404.

58. Karttunen, J., Sanderson, S., and Shastri, N. (1992). Detection of rare antigen-presenting cells by the lacZ T-cell activation assay suggests an expression cloning strategy for T-cell antigens. Proc. Natl. Acad. Sci. USA *89*, 6020–6024. https://doi.org/10.1073/pnas.89.13.6020.

59. Sancho, D., Mourão-Sá, D., Joffre, O.P., Schulz, O., Rogers, N.C., Pennington, D.J., Carlyle, J.R., and Reis e Sousa, C. (2008). Tumor therapy in mice via antigen targeting to a novel, DC-restricted C-type lectin. J. Clin. Invest. *118*, 2098–2110. https://doi.org/10.1172/JCI34584.

60. Garaude, J., Acín-Pérez, R., Martínez-Cano, S., Enamorado, M., Ugolini, M., Nistal-Villán, E., Hervás-Stubbs, S., Pelegrín, P., Sander, L.E., Enríquez, J.A., et al. (2016). Mitochondrial respiratory-chain adaptations in macrophages contribute to antibacterial host defense. Nat. Immunol. *17*, 1037–1045. https://doi.org/10.1038/ni.3509.

61. Christ, A., Günther, P., Lauterbach, M.A.R., Duewell, P., Biswas, D., Pelka, K., Scholz, C.J., Oosting, M., Haendler, K., Baßler, K., et al. (2018). Western diet triggers NLRP3-dependent innate immune reprogramming. Cell *172*, 162–175.e14. https://doi.org/10.1016/j.cell.2017.12.013.

62. Ramírez, F., Ryan, D.P., Grüning, B., Bhardwaj, V., Kilpert, F., Richter, A.S., Heyne, S., Dündar, F., and Manke, T. (2016). deepTools2: a next generation web server for deep-sequencing data analysis. Nucleic Acids Res. *44*, W160–W165. https://doi.org/10.1093/nar/gkw257.

63. Efremova, M., Vento-Tormo, M., Teichmann, S.A., and Vento-Tormo, R. (2020). CellPhoneDB: inferring cell-cell communication from combined expression of multi-subunit ligand-receptor complexes. Nat. Protoc. *15*, 1484–1506. https://doi.org/10.1038/s41596-020-0292-x.

64. de la Visitación, N., Robles-Vera, I., Toral, M., Gómez-Guzmán, M., Sánchez, M., Moleón, J., González-Correa, C., Martín-Morales, N., O'Valle, F., Jiménez, R., et al. (2021). Gut microbiota contributes to the development of hypertension in a genetic mouse model of systemic lupus erythematosus. Br. J. Pharmacol. *178*, 3708–3729. https://doi.org/10.1111/bph.15512.

65. Buenrostro, J.D., Wu, B., Chang, H.Y., and Greenleaf, W.J. (2015). ATAC-seq: A method for assaying chromatin accessibility genome-wide. Curr. Protoc. Mol. Biol. *109*, 21.29.1–21.29.9. https://doi.org/10.1002/0471142727.mb2129s109.

66. Kechin, A., Boyarskikh, U., Kel, A., and Filipenko, M. (2017). cutPrimers: A new tool for accurate cutting of primers from reads of targeted next generation sequencing. J. Comput. Biol. *24*, 1138–1143. https://doi.org/10.1089/cmb.2017.0096.

67. Langmead, B., and Salzberg, S.L. (2012). Fast gapped-read alignment with Bowtie 2. Nat. Methods *9*, 357–359. https://doi.org/10.1038/nmeth.1923.

68. Li, H., Handsaker, B., Wysoker, A., Fennell, T., Ruan, J., Homer, N., Marth, G., Abecasis, G., and Durbin, R.; 1000 Genome Project Data Processing Subgroup (2009). The Sequence Alignment/Map format and SAMtools. Bioinformatics *25*, 2078–2079. https://doi.org/10.1093/bioinformatics/btp352.

69. Heinz, S., Benner, C., Spann, N., Bertolino, E., Lin, Y.C., Laslo, P., Cheng, J.X., Murre, C., Singh, H., and Glass, C.K. (2010). Simple combinations of lineage-determining transcription factors prime cis-regulatory elements required for macrophage and B cell identities. Mol. Cell *38*, 576–589. https://doi.org/10.1016/j.molcel.2010.05.004.

70. Zhang, Y., Liu, T., Meyer, C.A., Eeckhoute, J., Johnson, D.S., Bernstein, B.E., Nusbaum, C., Myers, R.M., Brown, M., Li, W., et al. (2008). Model-based analysis of ChIP-Seq (MACS). Genome Biol. *9*, R137. https://doi.org/10.1186/gb-2008-9-9-r137.

71. Subramanian, A., Tamayo, P., Mootha, V.K., Mukherjee, S., Ebert, B.L., Gillette, M.A., Paulovich, A., Pomeroy, S.L., Golub, T.R., Lander, E.S., et al. (2005). Gene set enrichment analysis: a knowledge-based approach for interpreting genome-wide expression profiles. Proc. Natl. Acad. Sci. USA *102*, 15545–15550. https://doi.org/10.1073/pnas.0506580102.

72. Heger, A., Webber, C., Goodson, M., Ponting, C.P., and Lunter, G. (2013). GAT: a simulation framework for testing the association of genomic

intervals. Bioinformatics *29*, 2046–2048. https://doi.org/10.1093/bioinformatics/btt343.

73. Li, B., and Dewey, C.N. (2011). RSEM: accurate transcript quantification from RNA-Seq data with or without a reference genome. BMC Bioinformatics *12*, 323. https://doi.org/10.1186/1471-2105-12-323.
74. Ritchie, M.E., Phipson, B., Wu, D., Hu, Y., Law, C.W., Shi, W., and Smyth, G.K. (2015). limma powers differential expression analyses for RNA-sequencing and microarray studies. Nucleic Acids Res. *43*, e47. https://doi.org/10.1093/nar/gkv007.
75. Henriksen-Lacey, M., Bramwell, V.W., Christensen, D., Agger, E.-M., Andersen, P., and Perrie, Y. (2010). Liposomes based on dimethyldioctadecylammonium promote a depot effect and enhance immunogenicity of soluble antigen. J. Control. Release *142*, 180–186. https://doi.org/10.1016/j.jconrel.2009.10.022.

STAR★METHODS

KEY RESOURCES TABLE

REAGENT or RESOURCE	SOURCE	IDENTIFIER
Antibodies		
Anti-mouse CD16/CD32, clone 2.4G2	Tonbo Biosciences	Cat# 70-0161; RRID: AB_2621487
Biotin anti-mouse CD3 Antibody	Biolegend	Cat# 100244; AB_2563946
Biotin Rat Anti-Mouse CD45R/B220	BD pharmigen	Cat# 553086; AB_394615
Biotin Rat Anti-Mouse CD11b	BD pharmigen	Cat# 553309; AB_394773
Biotin anti-mouse Ly-6G/Ly-6C (Gr-1) Antibody	Biolegend	Cat# 108404; AB_313368
Biotin Anti-Mouse TER-119	Bionova	Cat# 30-5921;AB_2621651
PerCP/Cy5.5 anti-mouse CD115 (CSF-1R) Antibody	Biolegend	Cat# 135526; AB_2566461
anti-mouse CD45.2 V450	BD Bioscience	Cat# 560697; AB_1727495
PE Rat Anti-Mouse CD117	Fisher Scientific	Cat# 561075; AB_469430
Brilliant violet 650 anti-mouse CD11c	Biolegend	Cat# 117339; AB_2562414
Brilliant Violet 605™ anti-mouse CD150 (SLAM) Antibody	Biolegend	Cat# 115927; AB_11204248
Ly-6A/E (Sca-1) Monoclonal Antibody (D7), PE-Cyanine7	ThermoFischer	Cat# 25-5981-82; AB_469669
APC anti-mouse CD135 Antibody	Biolegend	Cat# 3007410; AB_1953264
APC/Cy7 anti-mouse CD48 Antibody	Biolegend	Cat# 3002191; AB_2561462
Brilliant Violet 570 anti-mouse CD45 Antibody	Biolegend	Cat# 103136; AB_10898325
Brilliant Violet 605™ anti-mouse/ human CD11b Antibody	Biolegend	Cat# 101237; AB_11126744
PE-Cy™7 Hamster Anti-Mouse CD11c	BD pharmigen	Cat# 558079; AB_647251
BV711 Rat Anti-Mouse F4/80	BD biosciences	Cat# 565612; AB_2734769
MHC Class II (I-A/I-E) Monoclonal Antibody (M5/114.15.2) Brilliant Ultra Violet™ 737	Invitrogen	Cat# 367-5321-82; AB_2896014
PE anti-mouse TNF-α Antibody	Biolegend	Cat# 506306; AB_315426
APC anti-mouse IL-6 Antibody	Biolegend	Cat# 504508; AB_10694868
biotin Anti-mouse Mincle, clone 1B6,	MBL	Cat# D266-3B; RRID: AB_10950261
Rat IgG1, Isotype Control Antibody, biotin, clone RTK2071	Biolegend	Cat# 400403; RRID: AB_326509
Anti-human IgG Fc, PE, polyclonal	eBiosciences	Cat# 12-4998-82; RRID: AB_465926
Chemicals, peptides, and recombinant proteins		
DNase I, Bovine Pancreas, > 2000U/MG	Biomatik	Cat# A4193
Liberase™ TL Research Grade	Sigma-Aldrich	Cat# 5401020001
Red Blood Cell Lysing Buffer Hybri-Max™	Sigma-Aldrich	Cat# R7757
2-Deoxy-D-glucose	Sigma-Aldrich	Cat# D8375
Vancomycin hydrochloride	Sigma-Aldrich	Cat# SBR00001
Metronidazole	Alfa Aesar	Cat# H60258
Neomycin trisulfate salt hydrate	Sigma-Aldrich	Cat# N1876
Ampicillin	Thermo Fisher BioReagents	Cat# BP1760-25
Amphotericin B	Fisher scientific	Cat# SV30078.01
Dextran sulfate Sodium	Alfa Aesar	Cat# J63606.22
LPS-EK	Invivogen	Cat# tlrl-eklps
Pam3CysK4	Invivogen	Cat# tlrl-pms
CpG ODN 1826	Invivogen	Cat# tlrl-1826-1
5′-methylthioadenosine	MedChemExpress	Cat# HY-16938
R406	Labclinics S.A.	Cat# SYN-1121-M001

(*Continued on next page*)

Continued

REAGENT or RESOURCE	SOURCE	IDENTIFIER
Rapamycin Ready Made Solution, 2.5 mg/mL in DMSO (2.74 mM)	Sigma-Aldrich	Cat# R8781
BRD5529	MedChemExpress	Cat# HY-115497
β-glucan	Biothera	Cat# F3005
Trehalose-6,6-dibehenate (TDB) Mincle Agonist	Invivogen	Cat# tlrl-tdb
Phorbol 12-myristate 12-acetate (PMA)	Sigma-Aldrich	Cat# P8139
Ionomycin calcium salt	Sigma-Aldrich	Cat# I0634
Mincle (Clec4e)-human Fc Chimera protein	Iborra et al.[32]; this paper	N/A
TMB Stop solution	SeraCare	Cat# 5120-0075
RPMI Medium 1640	Gibco	Cat# 11875093
PFA 16% (W/V)	Thermo Fisher BioReagents	Cat# 28908
Oligomycin A	Sigma-Aldrich	Cat# O4876
Carbonylcyanide-4-(trifluoreomethoxy) phenylhydrazone (FCCP)	Sigma-Aldrich	Cat# C2920
Rotenone	Sigma-Aldrich	Cat# R8875
Antimycin A	Sigma-Aldrich	Cat# A8674
Zymosan	Invivoge	Cat# tlrl-zyn
Chlorophenol red-β-D-galactopyranoside (CPRG)	Roche	Cat# 10884308001
AMPure XP beads	Beckman	Cat# A63880
EZ-Tn5 Transposase	Bionova cientifica	Cat# TNP92110
Columbia 5% SG horse	Biomerieux	Cat# 43050
PVX Chocolate polyvitex	Biomerieux	Cat# 43109
Mac Conkey	Biomerieux	Cat# 43149
GBS modified agar medium	Scharlau	Cat# 064-PA2117
Aesculin agar	Oxioid	Cat# OXOICM0888B
Triton X-100	Sigma-Aldrich	Cat# X100
LB agar plate	Fisher scientific	Cat# 10311141
Zymobiomics Microbial Community DNA	Zymo	Cat# D6305
Streptavidin magnetic beads	Miltenyi	Cat# 130-048-101
Dimethyl-dioctadecyl-ammonium bromide (DDA)	Sigma-Aldrich	Cat# D2779
Brilliant Violet 711™ Streptavidin	Biolegend	Cat# 405241
Brilliant Violet 421™ Streptavidin	Biolegend	Cat# 405226
CellTrace™ Violet	Invitrogen	Cat# C34557
CellTrace™ CFSE Cell Proliferation Kit	Invitrogen	Cat# C34554
LIVE/DEAD™ Fixable blue, for ultraviolet excitation	Thermofisher	Cat# L34962
LIVE/DEAD® Fixable Aqua Dead Cell Stain Kit, for 405 nm excitation	Thermofisher	Cat# L34957
Phospho-S6 Ribosomal Protein (Ser235/236) (D57.2.2E) XP® Rabbit mAb (PE Conjugate)	Cell signalling	Cat# 5316
Critical commercial assays		
RNeasy Micro Kit	QIAGEN	Cat# 74004
Seahorse XFe96 FluxPak mini	Agilent technologies	Cat# 102601-100
QIAamp PowerFecal (pro) DNA kit	QIAGEN	Cat# 51804
Mouse TNF DuoSet	R&D Systems	Cat# DY410
Mouse IL-6 DuoSet	R&D Systems	Cat# DY406
Human TNF-alpha DuoSet ELISA	R&D Systems	Cat# DY210
Human IL-6 DuoSet ELISA	R&D Systems	Cat# DY206
Sequal Prep normalization kit	Invitrogen	Cat# A1051001
API 20 strep test	Biomerieux	Cat# 20600
iDeal CUT&Tag kit for Histones	Diagenode	Cat# C01070021

(*Continued on next page*)

Continued

REAGENT or RESOURCE	SOURCE	IDENTIFIER
H3K4me3 Antibody	Diagenode	Cat# C15200152
Antibody package for CUT&Tag (anti-mouse) 24 rxns	Diagenode	Cat# C01070023
24 UDI for Tagmented libraries	Diagenode	Cat# C01011034
Deposited data		
RNAseq of GMP from mice treated with DSS, HK-EF or its excipient	https://www.ncbi.nlm.nih.gov/geo/	GSE281376
ATAC-Seq of GMP from mice treated with DSS, HK-EF or its excipient	https://www.ncbi.nlm.nih.gov/geo/	GSE230337
Cut&Tag of GMP from mice treated with DSS, HK-EF or its excipient	https://www.ncbi.nlm.nih.gov/geo/	GSE281375
Experimental models: Organisms/strains		
Mouse: *Clec4e*$^{-/-}$ *(B6.Cg-Clec4etm1.1Cfg)*	Wells et al.[57]	MGI ID: 5052164
Mouse: *Rag1*$^{-/-}$ *mice (B6.129S7-Rag1tm1Mom/J)*	N/A	MGI ID: 002216
Software and algorithms		
Analysis code for the study "————————"	https://zenodo.org/	N/A
GraphPad Prism version 9	GraphPad Software	https://www.graphpad.com/
FlowJo v10	Tree Star	https://www.flowjo.com/
BD FACSDiva™ Software	BD Biosciences	https://www.bdbiosciences.com/
Seahorse Wave Desktop Software	Agilent technologies	https://www.agilent.com/
Other		
LS Columns	Miltenyi Biotec	Cat# 130-042-401

EXPERIMENTAL MODEL AND STUDY PARTICIPANT DETAILS

Mice

Mice were bred and maintained in groups of 5 animals per cage at the CNIC under specific pathogen-free conditions. Unless otherwise stated, males of 6-8 weeks old were used. Animal studies were approved by the local ethics committee. The local ethics committee approved all animal studies (PROEX 236/16; PROEX 301.5/21; PROEX 302.6/21) and all animal procedures conformed to EU Directive 2010/63EU and Recommendation 2007/526/EC regarding the protection of animals used for experimental and other scientific purposes, enforced by Spanish law under Real Decreto 53/2013. Colonies included C57BL/6J (Jackson Laboratory); C57BL/6J male germ-free (GF) mice (University of Granada, Granada, Spain); *Clec4e*$^{-/-}$ (B6.Cg-Clec4etm1.1Cfg) mice were kindly provided by the Scripps Research Institute, through R. Ashman and C. Wells (Griffiths University, Australia)[57]; Rag1$^{-/-}$ mice (B6.129S7-Rag1tm1Mom/J, The Jackson Laboratory).

Cell lines

The L929 cell line (ATCC® CCL-1TM), used to produce M-CSF supernatant, was grown on 175 cm^2 cell culture flasks (Stemcell) and resuspended in Complete RPMI minus HEPES. Supernatants were obtained by filtering L929 culture supernatant at day 15 through 0.22 μm Stericup Filter units (Merck Millipore) and were used to subsequently supplement the medium for the generation of bone marrow derived macrophages.

Parental B3Z cells were kindly provided by N. Shastri, University of California) and expressed a β-gal reporter for nuclear factor of activated T cells (NFAT).[58] Parental B3Z cells were transduced with retroviruses encoding a chimera of the extracellular domain of either mouse Mincle, Dectin-1 or Dectin-2 fused to the transmembrane region from NKRP1B and the intracellular tail of CD3ζ followed by an internal ribosome entry site (IRES) sequence and the GFP gene.[59] In addition, B3Z cells were transduced with retroviruses encoding for FcRγ chain, Syk and mouse Mincle, to test signaling through the natural receptor.[32] Binding of ligands can be detected by NFAT reporter activation and induction of β-gal activity.[31]

Differentiation, culture, and stimulation of BMDMs

Murine BMDMs were generated as previously described[60] with some modifications. BM cells from WT C57BL/6J, *Clec4e* $^{-/-}$, *Rag1*$^{-/-}$, or C57BL/6J Germ-free mice, were cultured in Complete RPMI supplemented with 30% M-CSF (obtained from L929 cell supernatants) during 5 days in sterile, but not tissue-culture treated, 10cm Petri dishes. BMDMs, obtained from CTR or DSS pretreated mice, were plated in equal numbers (10^5 cells per well) in 96-well plates (200μl final volume, Corning) and rested overnight. BMDMs were then stimulated with TLR-ligands for 24 hours: LPS-EK (10ng/ml; TLR4 ligand), Pam3CSK4 (P3C4, 10ng/ml; TLR1/2 ligand) or CpG

(10μM; TLR9 ligand). Subsequently, supernatants were collected for cytokine analysis. In separate experiments, BMDMs obtained from C57BL/6 mice were primed with heat killed (80°C-15min) HK-EF ($2x10^2$ CFU/mL) for 24 hours. In the indicated experiments, BMDMs were pre-treated with 5′-methylthioadenosine (MTA) (500 μM), rapamycin (10nM), Syk Inhibitor (R406 (1μM)) or Card9 inhibitor (BRD5529 (10 μM)) one hour before HK-EF addition. In addition, to test other Mincle ligands cells were pre-treated with live-EF, HK-S. *aureus*, HK-*E.coli* ($2x10^2$ CFU/mL), $GlcC_{14}C_{18}$, $ManC_{14}C_{18}$ (1nM, kindly provided by Jérôme Nigou)[34] and enriched *Lactobacillus plantarum* mucus, obtained as previously reported.[16]

Human peripheral blood mononuclear cell isolation

Healthy donors were recruited from the Blood Donor Service of La Paz University Hospital. Peripheral blood mononuclear cells (PBMCs) from healthy donors were isolated from venous blood collected in EDTA-containing tubes using Ficoll-Plus (GE Healthcare Bio-Sciences) solution according to the manufacturer's instructions. PBMCs were washed twice with phosphate buffer saline (PBS), counted using Trypan blue staining, and resuspended at $2x10^6$ cell/mL in RPMI-1640 (Gibco) supplemented with 0.01% penicillin/streptomycin (p/s) (Thermofisher; Waltham, MA, United States) and with 10% FBS (Gibco). PBMCs ($6x10^6$ cells) were plated in 6-well plates with RPMI supplemented with 10% FBS and 0.01% penicillin/streptomycin (p/s) (Thermofisher; Waltham, MA, United States) and rested an overnight before stimulation.

METHOD DETAILS

DSS models

6-8-week-old male mice were treated (DSS) or not (CTR) in drinking water with dextran sulfate sodium (DSS) 36–55 KDa 3% w/v for 5 days, after a 5-day rest the mice were sacrificed. All mice were fed with standard chow for the whole experiment. The disease activity index (DAI) was evaluated after 10 days for each animal according to the scores listed in the Table below. Where indicated, mice were co-treated in the drinking water with antibiotics-fungizone cocktail (Vancomycin (0.5g/L), Metronidazole (1g/L), Neomycin (1g/L), Ampicillin (1g/L) and Amphotericin B (50mg/L).

SCORE	WEIGHT	Blood in feces	Stool formation
0	no change	-	normal
1	decrease by 1%	+	soft but formed
2	decrease by 3%	Blood visible	very soft
3	decrease by 5%	Bleeding out	diarrhea

Isolation and *ex vivo* stimulation of murine bone marrow cells

Bone marrow was isolated from femora and tibiae of 8 to 10-week-old male mice on WT C57BL/6J background kept in specific pathogen free (SPF) or Germ-free (GF) conditions, or $Clec4e^{-/-}$, or $Rag1^{-/-}$ kept in SPF. Bone marrow cell suspensions were prepared as described.[61] Briefly, bones were flushed with Roswell Park Memorial Institute medium (RPMI)-1640 supplemented with 10% Fetal Bovine Serum (FBS), 2mM L-glutamine, 100μg/ml penicillin, 100μg/ml streptomycin (all from Gibco), 10mM HEPES (Thermo Fisher), 1nM sodium pyruvate (Lonza), 100μM non-essential amino acids, herein referred to as "Complete RPMI". Cells were centrifuged at 4 °C (5 min; 350xg). Erythrocytes were lysed by resuspending the pellet in red blood cell lysis buffer (150mM NH_4Cl; 10mM $KHCO_3$; 130μM ethylenediaminetetraacetic acid (EDTA)). The reaction was stopped by adding RPMI and cells were again centrifuged and used directly. For *ex vivo* stimulation, total cells from BM were cultured in a 96-well flat-bottom plate (10^5 cells/well) in complete RPMI medium. After a 2-hour resting period in the incubator (37°C, 5% CO_2), cells were stimulated with TLR-ligands for 6 hours: LPS (10ng/ml; TLR4 ligand), Pam3CSK4 (P3C4, 10ng/ml; TLR1/2 ligand), and CpG (10μM; TLR9 ligand) and supernatants were collected for cytokine analysis.

Trained immunity protocol *in vitro*

HK-EF ($2x10^2$ CFU/mL) or particulate β-glucan (5μg/mL) were added to the cell culture medium for 24 hours to induce training; cells were then washed with PBS and fresh media was added. 5 days post-training, the medium was removed and LPS-EK was added in Complete RPMI, and supernatant was collected 24 hours after.

Trained immunity protocol *in vivo*

HK-EF ($2x10^2$ CFU) or PBS were injected i.v. at day 0. After 10 days or 8 weeks mice were challenged i.p. with 5μg LPS-EK or LPS-B5 respectively. In other set of experiments a dose-response curve was performed with a range of doses of HK-EF between $2x10^1$-$2x10^7$ and, after 10 days, mice were challenged i.p. with LPS-EK 5μg. One hour after LPS-EK challenge blood was obtained and TNF or IL-6 was measured by ELISA using Mouse TNF DuoSet; or IL-6 Mouse IL-6 DuoSet; R&D Systems, respectively in plasma according with the manufacturer instructions.

Flow cytometry analysis of bone marrow progenitors

For the analysis of bone marrow progenitor cells, single cell suspensions from BM were collected as described above. Cells were labelled with a viability staining Aqua dead cell stain kit (Thermofisher) 30 min. Then a cocktail of biotinylated antibodies against lineage (lin) markers CD3, B220, Cd11b (1:100), Gr-1 and TER-119 (1:20) all from BD Pharmigen for 20 min. Then, cells were additionally stained with MHCII-FITC (BD Pharmigen); CD115-PerCP (Biolegend); CD45.2-V450 (BD Biosciences); c-kit-PE (Biolegend); CD11c-BV650 (Biolegend); CD150-BV605 (Biolegend); Strep-BV711 (Biolegend); Sca1-PECy7 (Biolegend); CD135-APC (Biolegend); CD48-APCCy7 (Biolegend) (1:200) for 20 min. CMPs were identified as as lin− Sca1− c-kit+ CD48+ CD150+; GMPs were identified as lin− Sca1− c-kit+ CD48+ CD150-; MPP3 cells were identified as lin- Sca1+ c-kit+ CD135-CD150-CD48+. Samples were analyzed on the LSR Fortessa (BD), and quantification was performed using FlowJo software (TreeStar Inc).

mTOR activation by Phospho-S6 staining

Cultured BMDMs from C57BL/6 or Clec4e$^{-/-}$ mice were plated in equal number (6x10^5 cells per well) in 6-well plates (2000-μl final volume, Corning) and rested overnight. Cells were treated *in vitro* with HK-EF 2x10^2 CFU/mL, TDB 10 μg/mL or PBS (CTR). Some cells were also co-incubated with Rapamycin (10nM). After 24h cells were collected and labelled with Phospho-S6-PE (Cell Signalling #5316) according to the manufacturer protocol, activation was measured by flow cytometry MFI.

Quantification of cytokines

Cell culture supernatants and plasma samples were used to analyze cytokine production. TNF measurement by ELISA using Mouse TNF DuoSet; R&D Systems and IL-6 by ELISA using Mouse IL-6 DuoSet; R&D Systems to BMDMs or plasma from mice and Human TNF-alpha DuoSet ELISA; R&D Systems or Human IL-6 DuoSet ELISA; R&D Systems to PBMC following manufacturer's instructions

Bone marrow graft

WT C57BL/6J CD45.1$^+$ mice were irradiated with two doses of 550 rads (5.5 Gy), separated by at least 3 hours, for a total radiation dose of 1100 rads. After 2 hours, irradiated mice received BM cells extracted from the medulla of CD45.2$^+$ treatment group or control mice 1:1. Grafted mice received at least 2x10^6 BM cells in 100 ul PBS or 5x10^5 GMPs by i.v. injection, and antibiotics (100 mg/mice Ampicillin) were injected subcutaneously. To isolate GMPs, BM cells were stained as describe above and GMPs were identified as Lin-c-kit+sca-1-CD48+CD150- cells. After 30 days the reconstitution efficiency was checked in blood by analyzing CD45.1 vs CD45.2 expression. After 60 days mice were challenged *in vivo* with LPS 5μg and sacrificed after 1 hour. Blood was collected in EDTA-containing tubes to obtain plasma for cytokine analysis. Some mice were not injected with LPS to collect bone marrow as described above to analyze bone marrow progenitor cells. WT C57BL/6J CD45.1$^+$ mice were lethally-irradiated as described above. After 2 hours, irradiated mice received BM cells extracted from WT C57BL/6J or *Clec4e*$^{-/-}$ mice. After resting period mice were treated with DSS and disease index activity, and training was analyzed.

In another set of experiments, WT C57BL/6J CD45.1$^+$ mice irradiated as described before were grafted with BM from WT C57BL/6J or *Clec4e*$^{-/-}$ mice treated or not with DSS/HK-EF. After 60 days, recipient mice were challenged with 1.5x10^5 CFU per mouse *C.albicans* i.v. Survival and weight loss was analyzed.

Analysis of bacterial translocation

Liver and BM from DSS, ABX-treated, or untreated mice were homogenized in endotoxin-free PBS with 0.1% Triton X-100 to release intracellular bacteria. After a short centrifugation, 100μl supernatant from 1mL was added to a LB agar plate (Hardy Diagnostics) and cultured at 37°C for 24 hours in aerobic or anaerobic conditions. The number of colonies was counted and calculated as colony-forming units (CFU) per ml. BM treated as describe above was also used to analyze the bacterial translocation by 16S. Total genomic DNA was extracted from BM tissue with QIAamp PowerFecal (pro) DNA kit (QIAGEN-#51804) according to the manufacturer's instructions. Samples were disrupted using PowerBead Pro Tubes included in the kit in a TissueLyser II for 10 min at 30 Hz. The PowerBead Pro Tubes contained large beads. Then the DNA was purified following manufacturer's instruction and 16S performed. Briefly, for library preparation and sequencing, mock community DNA was included as positive control for library preparation (Zymobiomics Microbial Community DNA, ZymoResearch, Irvine, CA, USA) and to ensure quality control. Also, Negative controls of DNA extraction and PCR amplification steps were routinely performed in parallel, as well as positive controls, using the same conditions and reagents, to sure that no contaminant were introduced in any step. Samples were amplified using 16S rRNA V3-V4 regions specific primers (Forward; 5′TCGTCGGCAGCGTCAGATGTGTATAAGAGACAGCCTACGGGNGGCWGCAG-3′, Reverse;5′GTCTCG TGGGCTCGGAGATGTGTATAAGAGACAGGACTACHVGGGTATCTAATCC-3′). The PCR was performed in 10-μl volume with 0.2-μM primer concentration. Cycling conditions were initial denaturation of 3 min at 95 °C followed by 25 cycles of 95 °C for 30 s, 55 °C for 30 s, and 72 °C for 30 s, ending with a final elongation step of 5 min at 72 °C. PCR reactions were purified using AMPure XP beads (Beckman Coulter) with a 0.9× ratio according to manufacturer's instructions. PCR products were eluted from the magnetic beads with 32 μl of Milli-Q water and 30 μl of the eluate were transferred to a fresh 96-well plate. The primers contain overhangs allowing the addition of full-length Nextera adapters with barcodes for multiplex sequencing in a second PCR step, resulting in sequencing ready libraries with approximately 450 bp insert sizes. 5 μl of the first amplification were used as template for the second PCR with Nextera XT v2 adaptor primers in a final volume of 30 μl using the same PCR mix and thermal profile as for first PCR but only 8 cycles. After the second PCR, 25 μl of the final product was used for purification and normalization with SequalPrep normalization kit (Invitrogen), according to manufacturer's protocol. Libraries were eluted in 20 μl volume and pooled for sequencing. Sequencing

was performed in an Illumina MiSeq with 2×300 bp reads using v3 chemistry with a loading concentration of 10 pM. In all cases, 15% of PhIX control libraries was spiked in to increase the diversity of the sequenced sample. High-quality 16S rRNA amplicon sequences were analyzed via TADA (Targeted Amplicon Diversity Analysis using DADA2, implemented in Nextflow). The data set for mapping is from Green Genes (13.8), being forward and reverse truncate length 291/280 bp, ang maximum expected error 2. The Microbiome Analyst pipeline[62,63]was used for downstream analysis. The feature filter was manually performed removing taxa found in any of Negative controls of DNA extraction and PCR amplification and in germ free mice. The data were scaled by total sum scaling (TSS). GraphPad Prism 9 were used to analyze and illustrate the data.

Germ-free mice inoculation

Male Germ-free mice were colonized with whole gut microbiota from conventional C57BL/6. For this, fresh feces were collected, re-suspended in sterile PBS 1/20 w/v, centrifuged at 30xg for 10 min and kept -80°C until use)[64] Mice colonized were maintained in separate isolators for the duration of the experiment.

Germ-free mice mono-colonization

Isolated *E. faecalis cultured* as described above, was used to mono-colonize male Germ-free mice. The colonization was performed by oral gavage (100μl) for two consecutive days with 10^8 CFU of live bacteria. 24 hours after the second dose, DSS treatment was carried out as was described above. Mice colonized were maintained in separate isolators for the duration of the experiment.

Bacteria identification

Bacterial identification was performed using several tests. Isolated bacteria were grown in Columbia 5% SG horse (Biomerieux), PVX Chocolate polyvitex, (Biomerieux) Mac Conkey, (Biomerieux) GBS modified agar medium (VWR) and Aesculin agar (Oxoid). After 24 hours incubation at 37°C 5% CO_2, grown bacteria were analyzed by microbiological test, Gram staining (allows bacteria to be differentiated according to their cell wall) and catalase test following standard procedures. After, API 20 strep test (Biomerieux) was carried out following manufacturer's instructions.

The fermentation tests were inoculated with an enriched medium which rehydrates the sugar substrates. Fermentation of carbohydrates was detected by a shift in the pH indicator.

The reactions were read according to the Reading Table (included in the protocol) and the identification was obtained by referring to the Analytical Profile Index or using the identification software.

To confirm the bacterial species, Matrix-Assisted Laser Desorption Ionization Time-of-Flight (MALDI-TOF) and sequencing of the 16S were used. MALDI-TOF is a mass spectrometry technique to assess the unique "molecular fingerprint" of an organism. Briefly, an isolated colony was transferred with an inoculation loop and placed in a well of the plate, once it was dry, 1μl of 70% formic acid was added. When the sample was dry, 1μl of Bruker matrix solution (α-Cyano-4-hydroxycinnamic acid, HCCA) was added on the sample, and once dry, the plate was inserted into the MALDI BioTyper (Bruker Daltonics) for the identification. Spectra was analyzed by the BioTyper program (Bruker Daltonics, Inc) utilizing both the Bruker database and a previously created Inmunotek in-house database. The MALDI-TOF Biotyper system (Bruker Daltonics) provides a numerical score for the interpretation of results. Scores are classified globally into several categories. According to the manufacturer, the score thresholds for microorganism identification are currently as follows: a score of $\geq$1.80 represents high confidence and it is accepted for bacterial identification. The bacterial test standard (BTS) will be included as a positive quality control for all experiments.

The 16S was performed in collaboration with Charles Rivers using AccuGENX-ID® BacSeq to identified bacteria and MLST AccuGENX-ST to know the strain.

Enterococcus faecalis culture

Isolated *E. faecalis* as was described above from BM of DSS treated mice, was grown in aerobic condition overnight 37°C in LB medium under agitation 200 rpm. Grown bacteria were pelleted at 8000 g for 10 min and quantified by optical density and serial dilution 1:100 on Agar LB.

Flow cytometry analysis of Spleen

Spleen was harvested in R10 medium (RPMI Medium 1640 (Gibco®). Spleen was digested for 10 min with 0.25 mg/ml Liberase TL (Roche) and 50 μg/ml DNaseI (Sigma Aldrich), after incubation time single cells solution was obtained after mechanical disintegration and filtered out 70 μm filters. For the analysis of spleen single cell cells were labelled with a viability staining Aqua dead cell stain kit (Thermofisher) 30 min. Then cells were stained with a cocktail of antibodies with CD45-BV570 (BD Pharmigen); CD11b-BV605 (Biolegend); CD11c-PECy7 (Biolegend); F4/80-BV711 (Biolegend); MHCII-UV737 (Biolegend); CD90-UV805 (Biolegend); B220-PerCP (Biolegend); Ly6G-Pacific blue (Biolegend) 1:200 for 20 min. For intracellular staining cell were fixed with PFA 4% 15 min and permeabilized with permeabilization buffer (BSA 1%, Saponin 0.1% in miliQ water) for 30min. After that time cells was washed and stained with cocktail of antibodies TNF-PE and IL-6-APC (1:50) for 1h. Samples were analyzed on FACSymphony (Becton Dickinson) and quantification was performed using FlowJo software (TreeStar Inc).

Seahorse assay

Real-time Extracellular Acidification Rate (ECAR) in BMDMs was determined with an XF-96 Extracellular Flux Analyzer (Seahorse Bioscience). BMDMs were plated in Seahorse Cell Culture Microplates at a density of 100,000 cells per well and left to attach overnight. In the case of TDB stimulated BMDMs, 10mg TDB was coated to the Seahorse plate 24 hours before BMDMs were plated. After 24 hours of TDB or HK-EF stimulation, culture media was replaced by Seahorse Assay Medium (DMEM, 100μg/ml penicillin, 100μg/mL streptomycin, 2mM glutamine, 25mM glucose, 1mM pyruvate) at pH 7.4. Four technical replicates were used for each condition.

Seahorse cartridges were hydrated overnight in distilled water and calibrated for 1 hour in Seahorse XF Calibrant solution in a non-CO_2-corrected incubator at 37°C. Seahorse assay was run using the Glycolysis Stress Test Protocol. For the Mito Stress Test the following compounds were added: Port A – oligomycin (2μM); Port B - carbonyl cyanide-4-(trifluoromethoxy) phenylhydrazone (FCCP) (0.5μM); Port C – rotenone + antimycin A (0.5μM). ECAR was analyzed at the beginning of the protocol with 3 measurements before inhibitor injection.

Fungal infections

Mice were i.v. infected with 100 μl of *Candida albicans* ($1.5x10^5$ CFU per mouse) or ($7.5x10^4$ CFU per mouse in *Rag1*$^{-/-}$), both diluted in sterile PBS. Mice were monitored for weight, general health, and survival, following institutional guidance. *Candida albicans* (strain SC5314, clinical isolate) was kindly provided by Prof. C. Gil (Complutense University, Madrid, Spain). The fungus was grown on yeast extract-peptone-dextrose (YPD)-agar plates (Sigma) at 30°C for 24 hours to maintain the degree of virulence. After 24 hours, the colony was grown in liquid YPD at 30°C for 24 hours under agitation. Fungal titer was quantified and resuspended in PBS for injection.

Phagocytosis assay

BMDMs were obtained from WT or *Clec4e*$^{-/-}$ DSS/HK-EF treated mice. BMDMs stained with were exposed to CFSE-labeled (2.5 μM) HK-*C.albicans* (HK-CA) for 15 min. After extensive washing, cells were recovered on ice with PBS-5mM EDTA. Trypsin-EDTA (0.25%) (Gibco) treatment was used to remove bound, not internalized, HK-CA particles prior to analysis by flow cytometry. BMDMs Percentage of engulfed HK-CA was determined as double positive cells for Cell Violet and CFSE.

Viral infection

Mice were i.n. infected with 50 μl of Influenza A virus (15 PFU per mouse) diluted in PBS, and mice monitored daily for weight, general health, and survival, following the institutional guidance. Influenza A/Puerto Rico/8/34 (flu PR8) virus was a gift from E. Nistal-Villán (San Pablo CEU University, Madrid, Spain).

B3Z reporter assays

Parental or B3Z cells stably transduced with Mincle (WT receptor, Syk and FcγR chain or Mincle-CD3ς chimera),[32] Dectin-1-CD3ς chimera or Dectin-2-CD3ς chimera were used. For generation of Dectin-1 and Dectin-2 CD3ς chimera, B3Z were transduced with a retrovirus encoding a chimera of the extracellular domain of mouse Dectin-1 or Dectin-2 fused to the transmembrane region of NKRP1B and the intracellular tail of CD3ς followed by an IRES sequence and the GFP gene, as described.[31] $2x10^5$ cells per well were plated in 96-well plates and incubated with plated TDB or Zymosan or *Candida albicans* as positive control, respectively. In addition, cells were exposed to plated HK-EF ($2x10^5$, $2x10^7$ and $2x10^9$ CFU/mL) or HK-SA ($2x10^9$ CFU/mL) and cultured in RPMI 1640 supplemented with 2 mM L-glutamine, 100 U/ml penicillin, 100 μg/ml streptomycin, 50 μM 2-mercaptoethanol, and 10% heat-inactivated fetal bovine serum (FBS) (all from Life Technologies, Carlsbad, CA) at 37°C. After overnight culture, cells were lysed in lysis buffer containing chlorophenol red-β-D-galactopyranoside (CPRG, Roche)-containing buffer. 1-4 hours later, LacZ activity was measured by absorbance in the supernatant, with O.D. 595 measured relative to a reference of O.D. 655 nm on a spectrophotometer (Benchmark Plus. Bio Rad).

Human Fc recombinant assay

Mincle-hFc, generated as described,[32] and control-hFc (R&D Systems) were prepared in 10% skimmed milk in PBS and incubated overnight at 4°C on a rotating wheel, washed three times and labeled with PE-conjugated goat anti-hFc antibody (eBioscience). Specific binding of Mincle was detected by PE-positive signal by flow cytometry. Human Mincle-Fc chimera was blocked with anti-human Mincle 2F2 clone (Sigma-Aldrich). An isotype matched antibody (clone GC323, mouse IgM) was used as a negative control (Sigma Aldrich).

ATAC-Sequencing

BM cells were isolated as described above. Lineage negative (Lin^-) cells were enriched by staining with a panel of biotinylated antibodies against lineage committed cells (CD3, CD45R, CD11b (1:100) Ter-119, Gr-1 (1:20), all from BD Pharmigen). After washing, cells were incubated with streptavidin magnetic beads (Miltenyi) and passed through LS columns (Miltenyi), the negative fraction was collected for further staining with Sca-1 (APC), c-kit (CD117; PE), CD48 (APCCy7), CD150 (BV650), Streptavidin (BV421) (1:200) antibodies and with the viability marker Hoechst 33258 prior to sorting by FACS Aria II. GMPs were identified as Lin^-c-kit^+ sca-1^{1-} $CD48^+$ $CD150^-$ cells. 30,000-50,000 flow sorted GMPs were collected in ice-cold Flow cytometry buffer, and immediately treated as described previously.[65] In brief, cells were spun down in 25 μl cold lysis buffer at 500g for 20 min at 4°C. Afterwards, the transposition reaction was started by adding Nextera's Tn5 Transposase in reaction buffer. The transposition reaction mix was incubated for

30 min at 37°C, DNA was purified using a Qiagen MinElute PCR purification kit. ATAC-Seq libraries were purified using a PCR purification MinElute kit (Qiagen). Afterward, AMPure XP beads (Beckman) were used for size selection of the libraries, which were subsequently quantified using a Qubit fluorometer (ThermoFisher Scientific). Libraries size and quality were assessed using a 2100 Bioanalyzer instrument (Agilent). Libraries were sequenced in paired-end reads (2×50) using a NextSeq 2000 System. (Illumina) at the Genomics Unit of the CNIC.

ATAC-Seq data analysis

Sequencing reads were pre-processed by means of a pipeline that used FastQC, to asses read quality, and Cutadapt[66] to trim sequencing reads, eliminating Illumina and Nextera transposase adapter contaminations, and to discard reads that were shorter than 30 bp. Resulting reads were then mapped against reference genome GRCm38/MM10 with a pipeline that used bowtie2[67] as aligner, Piccard to mark duplicate alignments, and samtools[68] to eliminate duplicate, chimeric and sub-optimally multi-mapped alignments, keeping only properly paired and mapped reads. Alignments against the mitochondrial genome or chromosome Y were also removed. The final number of correctly aligned, filtered read pairs was between 12 and 47 million. TSS enrichment values, calculated with HOMER's annotatePeaks function[69] had values between 31 and 39. Once filtered alignments had been obtained, peaks (accessible DNA regions) were called with MACS3,[70] using parameters "–nomodel –shift -100 –extsize 200", and "-q 0.05" as the false discovery rate cut-off. The numbers of peaks detected were between 97000 and 131000. Next, filtered alignments and peaks, in BAM and XLS formats, respectively, were processed with the R package DiffBind to define a consensus set of 154,415 peaks, representing the complete collection of accesible DNA regions detected in any condition. DiffBind was also used to calculate and normalize peak coverage across samples, and to identify differentially accessible regions (DARs) in pair-wise contrasts, using EdgeR as analysis method. The fraction of reads in peaks (FRiP score), as calculated by DiffBind, was between 0.58 and 0.73. The number of DARs (with $p < 0.01$) was between 1,474 and 56,012, depending on the contrast. DAR collections were annotated with HOMER[68] to calculate the association of peaks to various genomic features, to identify the closest gene for each peak and to perform functional enrichment analyses, and to identify enriched motifs. In order to perform additional functional enrichment analyses with GSEA,[71] peaks in the consensus peak set were associated to the corresponding closest genes with HOMER. Then, unique gene-peak pairs were defined for each contrast by keeping those pairs with the maximal absolute ATAC-Seq accesibility logFC value, as long as gene-peak distance was shorter than 1MB. Gene lists were finally used to perform functional enrichment analyses with GSEA preranked, using accesibility logFC values to sort gene lists. The association between DARs and promoters and proximal and distal enhancers as defined in ENCODE's candidate Cis-Regulatory Element collection (cCRE; http://genome.ucsc.edu/cgi-bin/hgTrackUi?db=hg38&g=encodeCcreCombined) was tested with GAT,[72] Genomic heatmaps were generated with deepTools2.[62] Other data manipulations and graphical representations were produced with R.

Cut&Tag Sequencing

BM cells were isolated as was described above for ATAC-Seq protocol.

To analyze H3K4me3 mark by Cut&Tag the iDeal CUT&Tag kit for Histones (Diagenode) was used following the manufacturer's instructions. Briefly, we performed the analysis with individual samples which 30,000 fresh cells were used per immunoprecipitation (3 biological replicates per condition) and 1 μg of anti-H3K4me3 antibody was add to each reaction. As positive and negative controls, 1 μg of anti-H3K27me3 and IgG antibodies were also included in the Antibody Package for CUT&Tag, were used to carried out positive and negative control of analysis. Immunoprecipitation reactions took place on a rotating wheel at +4°C overnight. The secondary antibody binding was performed by adding 100 μl of diluted secondary antibody added per reaction and incubated on a rotating wheel at room temperature for 45 min. Cells were wash two times with Complete CT Wash Buffer and the tagmentation reaction was carried out with 100 ul of 1/250 dilution of pA-Tn5 Transposase. Cut&Tag libraries were purified using a PCR purification MinElute kit Libraries size and quality were assessed using a 2100 Bioanalyzer instrument (Agilent). Afterward, AMPure XP beads (Beckman) were used for size selection of the libraries, which were subsequently quantified using a Qubit fluorometer (ThermoFisher Scientific). Libraries were sequenced in paired-end reads (2×50) using a NextSeq 2000 System. (Illumina) at the Genomics Unit of the CNIC.

Cut&Tag data analysis

Following a strategy that was similar to that applied for ATAC-Seq data processing, FastQC and Cutadapt were used to pre-process sequencing data from CUTnTAG experiments, bowtie2 was used to map resulting reads against reference genome GRCm38/MM10, Piccard to mark duplicate alignments, and Samtools to eliminate sub-optimally multi-mapped alignments, keeping only properly paired and mapped reads, even if they corresponded to duplicate alignments, and removing alignments against the mitochondrial genome or chromosome Y. The number of unique reads in filtered alignments was around 80% of the number of processed reads, and fragment length distributions showed a maximal value at around 200, and a 10-bp sawtooth periodicity. Peaks were then called with MACS3, using parameter "–keep-dup auto", and "-q 0.01" as the false discovery rate cut-off. The numbers of peaks detected were between 13 and 17 thousand. Filtered alignments and peak sets were then processed DiffBind to define a consensus set of 19,905 peaks, to calculate and normalize peak coverage across samples, and to identify differential peaks in pair-wise contrasts, using EdgeR. The numbers of differential peaks (with raw $p\_value < 0.05$) were between 717 and 2,833, depending on the contrast. The collections of differential peaks were annotated with HOMER, including the identification of the closest gene for each peak, and non-redundant gene-peak pairs were defined for each contrast by keeping those pairs with the maximal absolute CUTnTAG logFC

value and maximal gene-peak distance of 1MB. Gene lists were used to perform functional enrichment analyses with GSEA pre-ranked, using CUTnTAG logFC values to sort gene lists

RNA-Seq sequencing

BM cells were isolated and treated as described above for ATAC-Seq and Cut&Tag.

Total RNA was isolated from GMP (miRNeasy Micro Kit). Bulk RNAseq experiments were performed in the Genomics Unit of the CNIC. Libraries were prepared using the NEBNext Single Cell/Low Input RNA Library Prep Kit for Illumina (New England Biolabs) according to manufacturer's instructions. All libraries were sequenced in a Nextseq 2000 (Illumina). FastQ files for each sample were obtained using bcl2fastq v2 2.20 software (Illumina). The number of reads per sample was between 11 and 21 million.

RNA-Seq analysis

RNA-Seq data were processed by applying a pipeline that used FastQC and Cutadapt. Resulting reads were mapped against the reference transcriptome GRCm38.99 and gene expression levels were estimated with RSEM.[73] The percentage of aligned reads was above 85% for all samples. Expected expression counts calculated with RSEM were then processed with an analysis pipeline that used the Bioconductor package limma[74]for normalization (using TMM method) and differential expression testing, taking into account only those genes expressed with at least 1 count per million (CPM) in at least three samples. Changes in gene expression were considered significant if associated to Benjamini and Hochberg adjusted p-value < 0.05. The collections of differentially expressed genes were used as input for functional enrichment analyses with QIAGEN Ingenuity Pathway Analysis (IPA).

DDA:TDB liposomes

Liposomes were prepared as described previously.[75] Briefly, a 5mg/mL solution of dimethyl-dioctadecyl-ammonium bromide (DDA) and TDB (Trehalose-6,6-dibehenate) were prepared using as dissolvent chloroform/methanol (9:1 v/v). DDA solution (5mg/mL) and TDB solution (5mg/mL) were mixed in a ratio 5:1 w/w (DDA:TDB). The organic solvent was removed using a roto-evaporator followed by flushing with N_2 to form a thin lipid film on the bottom of a round-bottomed flask. The DDA:TDB complex was stored at -20°C. The lipid film was hydrated with 2mL of PBS and heating for 20 min at 60 °C to a final concentration of 2 mg/mL DDA and 0.25 mg/mL TDB and used immediately to inject 10μg per mice.

QUANTIFICATION AND STATISTICAL ANALYSIS

Mice were included in the studies in a blind manner and randomly assigned to receive or not DSS (1:1 simple randomization). The same procedure was used to allocate mice to different groups to be treated with HK-EF or PBS and DDA:TDB or DDA.

Sample size was calculated according to a previously performed pilot study to determine the DSS, and the infective dose of *C. albicans*. For the *C. albicans* experiments, we considered two independent study groups with a dichotomous primary endpoint represented by mortality. As statistical parameters we chose an anticipated incidence of 50% for one group and 20% for another one, an alpha error of 0.05 and a power of 0.8. In the experimental models, the distribution normality of data was evaluated with the Kolmogorov-Smirnov (KS) test. Differences in weight loss between HK-EF and PBS groups were compared using a two-way ANOVA test, followed by multiple comparisons corrected using Bonferroni statistical hypothesis testing. Survival curves were compared with log rank (Mantel-Cox) test. Two-tailed unpaired Student's t test was generally used to evaluate statistical significance between two conditions, except for experiments *in vitro* with BMDMs and human monocytes in which paired Student's t test was applied to compare results within the same cultures. Differences were considered significant at $P < 0.05$ (*$p < 0.05$; **$p < 0.01$; ***$p < 0.005$; ****< 0.001). (Prism 9, Graph-Pad Software). The statistical test used and the definition of n are indicated in figure legends.